







Tau protein liquid–liquid phase separation can initiate tau aggregation

The Harvard community has made this article openly available. [Please share](#) how this access benefits you. Your story matters

Citation	Wegmann, S., B. Eftekhazadeh, K. Tepper, K. M. Zoltowska, R. E. Bennett, S. Dujardin, P. R. Laskowski, et al. 2018. "Tau protein liquid–liquid phase separation can initiate tau aggregation." <i>The EMBO Journal</i> 37 (7): e98049. doi:10.15252/embj.201798049. http://dx.doi.org/10.15252/embj.201798049 .
Published Version	doi:10.15252/embj.201798049
Citable link	http://nrs.harvard.edu/urn-3:HUL.InstRepos:37067888
Terms of Use	This article was downloaded from Harvard University's DASH repository, and is made available under the terms and conditions applicable to Other Posted Material, as set forth at http://nrs.harvard.edu/urn-3:HUL.InstRepos:dash.current.terms-of-use#LAA

Tau protein liquid–liquid phase separation can initiate tau aggregation

Susanne Wegmann^{1,*†} , Bahareh Eftekharezadeh^{1,†}, Katharina Tepper^{2,†}, Katarzyna M Zoltowska¹, Rachel E Bennett¹, Simon Dujardin¹, Pawel R Laskowski³ , Danny MacKenzie¹, Tarun Kamath¹, Caitlin Commins¹, Charles Vanderburg¹, Allyson D Roe¹, Zhanyun Fan¹, Amandine M Molliex⁴, Amayra Hernandez-Vega⁵, Daniel Muller³ , Anthony A Hyman³, Eckhard Mandelkow^{2,6,7}, J Paul Taylor^{4,8} & Bradley T Hyman^{1,**} 

Abstract

The transition between soluble intrinsically disordered tau protein and aggregated tau in neurofibrillary tangles in Alzheimer's disease is unknown. Here, we propose that soluble tau species can undergo liquid–liquid phase separation (LLPS) under cellular conditions and that phase-separated tau droplets can serve as an intermediate toward tau aggregate formation. We demonstrate that phosphorylated or mutant aggregation prone recombinant tau undergoes LLPS, as does high molecular weight soluble phospho-tau isolated from human Alzheimer brain. Droplet-like tau can also be observed in neurons and other cells. We found that tau droplets become gel-like in minutes, and over days start to spontaneously form thioflavin-S-positive tau aggregates that are competent of seeding cellular tau aggregation. Since analogous LLPS observations have been made for FUS, hnRNPA1, and TDP43, which aggregate in the context of amyotrophic lateral sclerosis, we suggest that LLPS represents a biophysical process with a role in multiple different neurodegenerative diseases.

Keywords aggregation; Alzheimer's disease; liquid–liquid phase separation; phosphorylation; tau

Subject Categories Physiology; Protein Biosynthesis & Quality Control

DOI 10.15252/embj.201798049 | Received 18 August 2017 | Revised 17 January 2018 | Accepted 19 January 2018 | Published online 22 February 2018

The EMBO Journal (2018) 37: e98049

Introduction

Tau protein is the major constituent of neurofibrillary tangles in Alzheimer's disease (AD) and of various other forms of intracellular inclusions in frontotemporal dementias (FTDs). Tau is classically described as a soluble neuron-specific microtubule binding (MTB) protein; however, the connection between tau (mis)function and neurodegeneration is uncertain. It is clear, for example, that post-translational modifications (PTMs) and tau mutations predisposing to aggregation are both associated with neurodegeneration. Recently, soluble hyperphosphorylated high molecular weight tau was identified as a bioactive form, which can be released and taken up by neurons and initiate templated misfolding of cytoplasmic tau in neurons (Takeda *et al*, 2015). This soluble hyperphosphorylated tau is, however, clearly distinct from aggregated fibrillary tau in neurofibrillary tangles, despite both being implicated in tau toxicity. Tau is an exceptionally soluble protein, and the molecular mechanisms that link soluble tau to aggregated tau are unknown. We now report that tau—similar to several other neurodegenerative disease-associated proteins such as the prion-domain harboring RNA binding proteins FUS, TDP43, hnRNPA1 (King *et al*, 2012)—can undergo liquid–liquid phase separation (LLPS), and we suggest that this observation may provide a biological mechanism for tau aggregation in neurodegenerative diseases.

The longest isoform of tau in the human CNS contains a MTB region that contains four pseudo-repeats (R1–R4) plus flanking proline-rich regions (P1, P2, and P3; Gustke *et al*, 1994), a shorter (~40 aa) C-terminal tail, and a long (~250 aa) flexible N-terminal half of tau, which projects from the surface of microtubules in the MT-bound state (Goode *et al*, 1997), and forms a polyelectrolyte

1 Department of Neurology, Massachusetts General Hospital, Harvard Medical School, Charlestown, MA, USA

2 German Center for Neurodegenerative Diseases (DZNE), Bonn, Germany

3 Department for Biosystems Science and Engineering, ETH Zurich, Basel, Switzerland

4 Department of Cell & Molecular Biology, St. Jude Children's Research Hospital, Memphis, TN, USA

5 Max-Planck Institute for Molecular Cell Biology & Genetics, Dresden, Germany

6 Max-Planck Institute for Metabolism Research, Hamburg Outstation c/o DESY, Hamburg, Germany

7 CAESAR Research Center, Bonn, Germany

8 Howard Hughes Medical Institute, Chevy Chase, MD, USA

*Corresponding author. Tel: +1 617 230 7184; E-mail: swegmann@mgh.harvard.edu

**Corresponding author. Tel: +1 617 726 3987; E-mail: bhyman@mgh.harvard.edu

†These authors contributed equally to this work

brush around fibrillary aggregates of tau (Sillen *et al.*, 2005; Wegmann *et al.*, 2013). The lack of a fixed tertiary protein structure classifies tau as an intrinsically disordered protein (IDP). Proteins that contain intrinsically disordered regions often have multiple biological functions (Wright & Dyson, 2014), and some of them aggregate in protein aggregation diseases, such as huntingtin protein in Huntington's disease, α -synuclein in Parkinson's disease, TDP43 and FUS in ALS, and tau in Alzheimer's disease and tauopathies (Uversky *et al.*, 2008).

Recent studies revealed that the RNA binding and stress granule-associated proteins FUS (Patel *et al.*, 2015), hnRNPA1 (Molliex *et al.*, 2015), and TDP43 (Conicella *et al.*, 2016) have the ability to reversibly form intracellular membrane-less organelles. These reversible droplets represent physiologically active protein or protein-nucleic acid "bioreactors" (Hyman *et al.*, 2014), which form through a process known as LLPS (Brangwynne *et al.*, 2015). Such transient membrane-less organelles have multiple cellular functions, such as p-granule formation to establish intracellular gradients of RNA transcription (Brangwynne *et al.*, 2009), the enrichment of RNA binding proteins in stress granules (Lin *et al.*, 2015; Molliex *et al.*, 2015), concentrating transcription factors in nucleoli (Berry *et al.*, 2015), and the initiation of microtubule spindle formation (Jiang *et al.*, 2015). However, the functional phase separation of nuclear proteins was shown to be disrupted by C9orf72 GR/PR dipeptide repeats (Lee *et al.*, 2016) and is related to protein aggregation in neurodegeneration (Schmidt & Rohatgi, 2016).

In most cases, the phase transition of these proteins is driven by so-called low complexity domains (LCDs) in their sequence, a term of somewhat inconclusive nomenclature that is often used to describe protein domains of low amino acid variance leading to inhomogeneous charge distribution or polarity distribution along the peptide backbone (Nott *et al.*, 2015). For example, FUS, TDP-43, and hnRNPA1 contain "prion-like" LCDs that drive their phase separation. However, in the case of tau, no typical low complexity domain (LCD) exists in the protein sequence, but the intrinsic disorder and the inhomogeneous charge distribution of full-length tau (Lee *et al.*, 1988) led us to postulate that tau may undergo a similar phase separation. In fact, recent reports using recombinant tau constructs support the argument that tau, despite having no defined LCDs, can undergo LLPS facilitated by crowding agents or RNA *in vitro* (Ambadipudi *et al.*, 2017; Hernandez-Vega *et al.*, 2017; Zhang *et al.*, 2017).

We now show that full-length human tau protein can efficiently undergo LLPS to form condensed liquid tau droplets in cell physiological conditions. We observed the formation of tau droplets not only *ex vivo* for post-translationally modified recombinant tau, but also in neurons *in vitro* and with strong evidence even *in vivo*, using high molecular weight hyperphosphorylated tau isolated from human Alzheimer brain. Importantly, tau LLPS is enabled and regulated by physiological and pathological-like tau phosphorylation, by disease-associated mutations, and can be induced in *in vitro* aggregation conditions. Similar to FUS and hnRNPA1 proteins (Molliex *et al.*, 2015; Murakami *et al.*, 2015; Patel *et al.*, 2015), droplets of pathological tau "mature" through a viscous gel phase into protein aggregates; the tau aggregates become thioflavin-S positive, suggesting the emergence of the beta-pleated sheet conformation present in tau aggregates *in vivo*. It appears that the phase separation of tau at physiological protein concentrations may be catalyzed by an

interplay of electrostatic interactions in the unstructured N-terminal half of tau, combined with hydrophobic interactions of the C-terminal MTB domain, which can stabilize tau droplets possibly through β -sheet structures. These findings complement and provide additional biological relevance to the recent reports showing *in vitro* tau LLPS of repeat domain constructs at rather high concentrations (Ambadipudi *et al.*, 2017) and in the presence of aggregation triggering polyanionic RNA (Zhang *et al.*, 2017).

Together, our data strongly support the hypothesis that intracellular phase separation of tau leads to subcellular foci of high local concentration of tau, which may be important for physiological roles of tau, and—in the setting of aberrant phosphorylation or disease-relevant pro-aggregation mutations—lead to tau aggregation. By analogy to hnRNPA1 (Molliex *et al.*, 2015)-, TDP-43 (Conicella *et al.*, 2016)-, FUS (Murakami *et al.*, 2015)-, and C9orf72-derived dipeptide repeats (Lee *et al.*, 2016), tau LLPS could act to initiate tau aggregation in AD and FTD. We suggest that protein LLPS may be a biophysical mechanism underlying multiple protein aggregation and neurodegenerative diseases.

Results

Intrinsically disordered tau protein can accumulate in droplet-like assemblies in neurons

Several disordered proteins with LCDs have been shown to undergo LLPS leading to liquid droplet formation in aqueous solution upon increasing the molecular crowding in the solution (Mitrea *et al.*, 2016). Cells use LLPS to reversibly assemble membrane-less organelles such as stress granules, p-granules, or nucleoli (reviewed in Mitrea *et al.*, 2016; Hyman *et al.*, 2014). In a number of LLPS proteins, including Ddx4 (Nott *et al.*, 2014), domains of low amino acid complexity introduce an unequal charge distribution along the protein backbone resulting in multivalency of these polypeptides with alternating patches of high positive or negative charge densities (Toretsky & Wright, 2014). The phase separation of these proteins is often driven by electrostatic interactions within the LCDs, or between them. Tau is intrinsically disordered (Fig 1A, Appendix Fig S1), and the distribution of charges in the longest human isoform of tau (2N4R, 441 aa) at physiological pH 7.4 shows *per se* a similar multivalent pattern (Wegmann *et al.*, 2013): The N-terminus (\approx aa 1–120) has a negative net charge, the middle domain (\approx aa 121–250) has a large excess of positive charges, the repeat domain (TauRD, \approx aa 251–390) has a moderate excess of positive charges, and the C-terminus (\approx aa 391–441) is negatively charged (Fig 1B).

Based on this knowledge about the disorder and inhomogeneous charge distribution of tau, we postulated that human tau may also be able to undergo LLPS in neurons. To test this hypothesis, we expressed GFP-tagged full-length tau (GFP-tau441) in primary cortical mouse neurons. The expression of GFP-tau441 led to the formation of mobile intracellular droplet-like tau accumulations in the cytosol (Fig 1C, Movies EV1–EV3), and fluorescence recovery after photobleaching (FRAP) of intraneuronal GFP-tau441 droplets revealed a fast recovery rate with an immobile tau molecule fraction of \approx 30% (Figs 1D and EV1A). Some droplet-like tau accumulations in axons of neurons grown

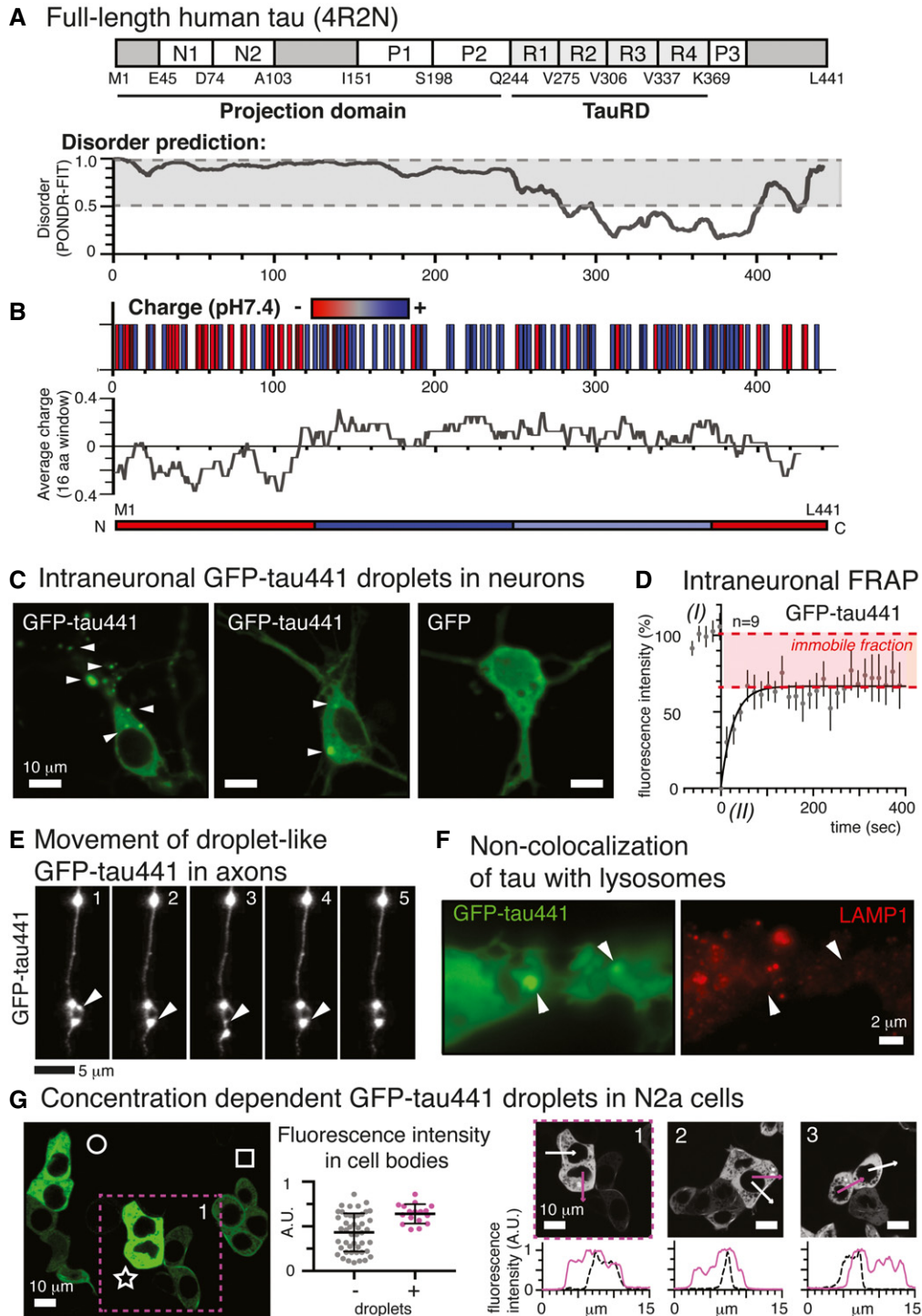


Figure 1.

in microfluidic chambers moved retro- as well as anterograde (Fig 1E, Movie EV4). Interestingly, GFP-tau441 droplets (Movies EV1–EV3) appeared less mobile compared to droplets formed by the N-terminal projection domain of tau441 (aa 1–256), GFP-tau256 (Movies EV5–EV7), maybe because of the ability of full-length GFP-tau441 but not GFP-tau256 to bind microtubules via the repeat domain.

We did not observe the fusion or fission of GFP-tau441 droplets in neurons, which can be seen as a typical behavior of liquid droplets. However, the observed FRAP recovery of the GFP-tau droplets excludes the possibility that the observed spherical droplets resemble large tau aggregates previously reported for mutant tau expressed in neurons (Hoover *et al*, 2010). Tau aggregates induced in HEK TauRDP301S-CFP/YFP cells, or GFP-polyQ aggregates in

Figure 1. Droplet-like condensation of intrinsically disordered human tau protein in neurons.

- A Protein sequence and disorder prediction (PONDR) of the longest human tau isoform [2N4R, 441 amino acids (aa)]. The highly disordered N-terminal half (projection domain) contains two N-terminal repeats (N1, N2) and two proline-rich regions (P1, P2). The repeat domain (TauRD) consists of four pseudo-repeats (R1–R4), can transiently adopt short stretches of β -strand structure in R2 and R3, facilitates microtubule binding together with P2 + P3, and mediates the aggregation of tau.
- B Single amino acid and average (sliding window of 6 aa) charge distribution along the tau441 sequence (at pH 7.4) reveal the following charged domains in tau441: the negatively charged N-terminal end (\approx aa 1–120), a strongly positively charged middle domain (aa 121–250), the positively charged TauRD (aa 251–400), and a negatively charged C-terminal end (aa 401–441).
- C Intracellular droplet-like accumulations of GFP-tau441 (white arrows) in primary cortical mouse neurons. Expression of GFP alone does not lead to droplets. Droplet dynamics in neurons is shown in Movie EV1.
- D FRAP reveals incomplete recovery of droplet-like tau in neuronal cell bodies indicating an immobile fraction of GFP-tau441 molecules of \approx 30%.
- E Neurons growing in microfluidic chambers extend their axons in microgrooves (Takeda et al, 2015). Time-lapse imaging (#1–5, time interval \approx 3 s) shows the movement of droplet-like GFP-tau441 (white arrows) in axons over time.
- F Immunofluorescent labeling of neurons expressing GFP-tau441 shows that tau accumulations (white arrows) do not co-localize with lysosomes (LAMP1).
- G In murine neuroblastoma cells (N2a) expressing GFP-tau441, droplet-like tau occurs in cells having a critical GFP-tau441 concentration (white star). In cells with low expression level (white square), GFP-tau binds to microtubule bundles; in cells with medium GFP-tau441 (white circle), excess GFP-tau441 fills the cell bodies. The graph shows the GFP fluorescence intensity in cell bodies with (pink) and without (gray) droplets. Cross-sectional profiles of cells with droplets suggest a similar tau concentration of GFP-tau on microtubules (white lines, black traces) and in droplets (pink lines and traces).
- Data information: In (D), data are presented as mean \pm s.e.m., $n = 9$ droplets; data have been fitted with a one-phase exponential fit, $r^2 = 0.08215$. In (G), average fluorescence intensity in cell bodies is plotted as mean \pm s.e.m., $n = 45$ for “– droplets”, $n = 17$ for “+ droplets”.

primary neurons, did not show recovery after photobleaching (Fig EV1B and C), whereas soluble GFP-tau in the cytosol and bound on microtubules showed fast recovery (Fig EV1D). Moreover, the expression of wild-type tau does not lead to intracellular tau aggregation, neither *in vitro* (Lim et al, 2014) nor *in vivo*. Furthermore, GFP-tau441 droplets did not co-localize with membrane-bound organelles like lysosomes (Fig 1F), endosomes (Appendix Fig S2A), or the endoplasmic reticulum (ER, Appendix Fig S2B).

Interestingly, when tau441 N-terminally fused to the fluorescent protein Dendra2, Dendra2-tau441, was expressed in the cortex of living wild-type mice upon stereotactical injection of AAV Dendra2-tau441 into the somatosensory cortex, two-photon imaging through a cranial window revealed a heterogeneous distribution of unconverted green Dendra2-tau441 with spherical droplet-shaped accumulations in the cell bodies of neurons in cortex layer 2/3 (Fig EV1E, neuron #1–3). Some of these accumulations also occurred along neuritic projections (Fig EV1E, #4–6). In contrast, the distribution of GFP in neurons of the control AAV GFP-injected hemisphere was

homogeneous in cell bodies and projections of transduced neurons. These data indicated that tau LLPS may also occur in the living brain.

Notably, in N2a cells, GFP-tau droplets could mostly be observed in cells with sufficiently high GFP-tau expression levels (Fig 1G), whereas in primary neurons, droplets could also occur in neurons with rather low or medium GFP-tau441 expression levels. This indicated that tau LLPS in neurons may be regulated by additional factors. In neurons, tau is phosphorylated at multiple sites (Fig EV1F; Iqbal et al, 2005). Many of tau's physiological and pathological phosphorylation sites are located in the positively charged middle domain of the N-terminal half and in the repeat domain (Johnson & Stoothoff, 2004), where phosphorylation causes a local increase or a change in domain charge from positive to neutral or negative, and hence can change intra- and intermolecular interactions of tau. However, most previous *in vitro* studies on tau aggregation utilized recombinant non-phosphorylated tau from *Escherichia coli*, and in these studies, tau LLPS has not been observed.

Figure 2. Liquid droplet characteristics of p-tau441.

- A Qualitative distribution of phosphorylation sites in p-tau441 [pS68/69, pT153, pT175, pT181, pS184, pS199, pS202, pT205, pS210, pT212, pS214, pT217, pT231, pS235, pS262, pS324, pY310, pS316, pS396, pS404, pS422 (Mair et al, 2016)]. The charge at pH 7.4 of domains in unphosphorylated tau441 is indicated as well.
- B Liquid–liquid phase separation (LLPS) of p-tau441 in presence of molecular crowding (12.5% w/v Ficoll-400). No phase separation is observed without crowding agent or in the absence of p-tau441 protein.
- C Liquid droplets formed by p-tau441 in the presence of 10% (w/v) PEG were negative stained with uranyl-acetate and visualized by transmission electron microscopy (TEM). p-tau441 droplets are decorated with gold particles after immunogold labeling using anti-tau antibody K9JA.
- D Shortly after formation (15 min), p-tau441 droplets stop to coalesce and often occur as doublets or triplets. With time (60 min), droplets grow in size but remain colloidal. Droplet fusion is shown in Movie EV1.
- E p-tau441 droplets (in buffer with 10% PEG) exhibit glass surface wetting properties characteristics for liquids.
- F Phase diagram of tau LLPS (p-tau441 concentration (μ M) versus PEG concentration (% w/v)).
- G In conditions modeling the intraneuronal environment (\sim 2 μ M tau, 10% PEG, pH 7.5), p-tau441 droplets can form at very high NaCl concentrations (up to 3 M NaCl) in the buffer. Guanidinium hydrochloride (GdmHCl) prevents p-tau441 LLPS at 3 M; at this concentration, tau aggregates become visible. The chaotropic salt sodium thiocyanate (NaSCN) can inhibit LLPS with increasing concentration, whereas droplets become larger in the presence of the kosmotropic salt ammonium sulfate ((NH₄)₂SO₄). Urea, which denatures proteins by unfolding secondary structures, prevents p-tau441 LLPS. $n = 3$ per condition, determined after 3 h.
- H Brightfield images for p-tau441 LLPS under different salt conditions graphed in (G).
- I The addition of 10% 1,6-hexanediol to p-tau441 droplets substantially reduced the amount of tau droplets formed.
- Data information: In (F) and (G), the phase diagrams show the average of three measurements.

Phosphorylated human full-length tau undergoes LLPS *in vitro*

We decided to describe the conditions for tau LLPS in more detail and produced recombinant full-length human tau (p-tau441, aa 1–441; Fig 2A) in Sf9 insect cells, which are able to introduce PTMs including phosphorylation into recombinant tau (Tepper *et al*, 2014). Previously, the phosphorylation sites found in

p-tau441 by mass spectrometry were reported to be similar to the phosphorylation of tau extracted from AD brains (Mair *et al*, 2016; Fig EV1G), with phosphorylation in the repeat domain (R1–R4), in the proline-rich region (P1 + P2), and some in the N-terminal insets (N1 and N2) of tau441 (Fig 2A). Here, we used Sf9 p-tau441 protein from the same source that was expressed and purified under identical conditions, and verified most of the

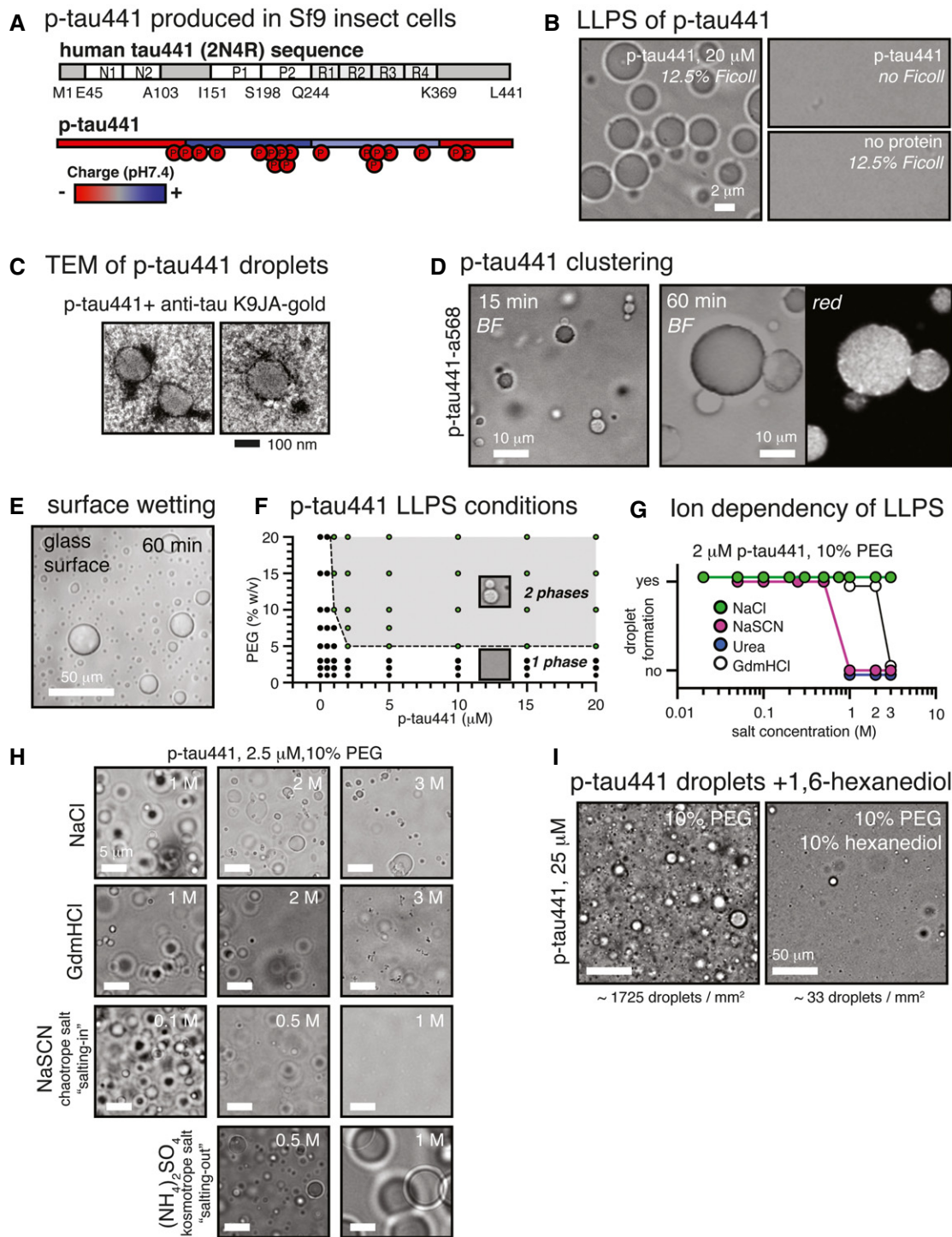


Figure 2.

reported phosphorylation sites in p-tau441 by Western blot analysis (Fig EV1G).

As hypothesized for LLPS proteins, we were able to observe the rapid formation of liquid p-tau441 droplets in solution upon the addition of crowding agents Ficoll (12.5% w/v; Fig 2B) or polyethylene glycol (PEG, 10% w/v; Fig EV2A) to mimic the intracellular crowding of ≈ 150 mg/ml proteins present in the cytosol. No droplets were observed for solutions of p-tau (2–10 μ M) without crowding agent and for crowding agent without tau protein (Fig 2B), or for crowding agent with control protein GFP at the same concentration (Fig EV2A). We verified that the observed phase-separated droplets contain tau protein by adding PEG to fluorescently labeled p-tau441-Alexa568, and show the integration of fluorescently labeled tau protein into the droplets (Fig EV2B). Analyzing the fluorescence intensity of ptau441-a568 droplets using confocal images, we measured an apparent p-tau441 concentration of $\approx 34.3 \pm 6.4$ μ M p-tau441 in the droplets and $\approx 3.6 \pm 0.3$ μ M remaining in the solution (mean \pm s.d.; 5 μ M p-tau441-a568 starting concentration and 10% PEG; Fig EV2B and C). This value does not consider fluorophore–fluorophore quenching and other effects caused by the highly crowded and viscous environment in the droplets and thus likely underestimates the actual droplet p-tau441 concentration. When using the crowding agent dextran to initiate p-tau441 LLPS, fluorescently labeled dextrans of different molecular weights (mean MW = 3, 20, and 70 kDa) remained excluded from the droplets, as indicated by confocal imaging (Fig EV2D). In contrast, monomolecular dyes with affinity to hydrophobic protein regions, such as thioflavin-S, methylene blue, and viscous aqua, immediately co-partitioned into the droplets (Fig EV2E); however, the dye fluorescence in the droplets may be further enhanced by the inhibition of free molecular rotation of the dye due to a higher viscosity in the droplets.

Interestingly, at very high p-tau441 concentration (50 μ M), spontaneous LLPS occurred at the outer edge of cover slip deposited solution droplets, where the protein concentration is highest due to evaporation and surface tension effects, even in the absence of crowding agents (Fig EV3A, Movie EV8). This indicates that tau phase separation depends on a critical local protein concentration. However, the concentration of p-tau441 in these droplets has to be higher than the starting concentration of 50 μ M, suggesting that the apparent droplet concentration we measured using fluorescently labeled p-tau441 in the presence of PEG (≈ 34 μ M) may underestimate the actual concentration by 30%. In solutions with the polymeric crowding agents Ficoll, PEG, and dextran, excluded volume effects can induce the critical concentration and trigger tau LLPS at lower tau solution concentrations. Indeed, we found that solutions of 10% (w/v) ethylene glycol and glucose, which are the monomeric analogs of PEG and dextran, failed to induce tau LLPS at the same concentrations (10% w/v crowding agent, 10 μ M p-tau441; Fig EV3B).

Tau forms stable droplets with initial liquid phase behavior

Tau droplets, when directly adsorbed onto electron microscopy grids right after preparation (Fig 2C), differed in size with diameters of ≈ 0.1 – 1.0 μ m and reached diameters up to ≈ 10 μ m when left in solution (Fig 2B). The tau droplets were mobile while in solution and, immediately after LLPS, able to coalesce (Movie EV9). After

15 min, however, the fusion of droplets was largely prevented (Fig 2D), and after longer incubation times (> 1 h), the droplets sunk down (likely driven by gravity due to higher protein density than the surrounding liquid phase) and coated the bottom glass surface (Fig 2E).

Next, we tested whether tau LLPS could occur at physiologically relevant tau concentrations, intracellular molecular crowding (≈ 50 – 400 mg/ml macromolecular density; Fulton, 1982), and electrolyte concentrations (≈ 100 – 200 mM; Lodish *et al*, 2000) conditions. The microscopic (i.e., visible in conventional light microscopy with a 63 \times objective) formation of p-tau441 droplets could be observed at PEG concentrations $\geq 5\%$ (\approx crowding of ≥ 50 mg/ml macromolecule density without tau protein) and at a critical protein concentration of ≈ 1.0 μ M (Fig 2G). Notably, the amount of tau needed for *in vitro* LLPS induced with the neutral molecule PEG likely differs from the tau concentration critical for LLPS in a neuron, because (i) the intraneuronal distribution of tau is highly heterogeneous (usually high in the axon and low in the soma and dendrites), (ii) different isoforms and post-translational modified and truncated forms of tau coexist, (iii) the pool of free soluble tau released from microtubules is highly dynamic depending on phosphorylation, and (iv) multiple other binding partners of tau have been identified that could deplete tau from the free soluble pool available for LLPS. Recently, it has also been shown that the usual distribution of tau in neurons can be changed upon exposure to A-beta, which can induce the local transcription of tau in dendrites as well (Zempel & Mandelkow, 2015; Li & Götz, 2017).

However, early studies performed on neuronal cells (Drubin *et al*, 1985) suggested an intracellular tau concentrations of 1–3 μ M. Furthermore, a tubulin concentrations of $\approx 3\%$ total protein (≈ 20 μ M tubulin; Hiller & Weber, 1978), average [tubulin: tau] ratios of $\approx [17:1]$ (Drubin *et al*, 1985), and 30–50% of unbound free tau (Ackmann *et al*, 2000) have been reported; from these numbers, a tau protein concentration of ≈ 0.5 – 2 μ M appears to be a reasonable estimate. In addition, we performed new experiments on human cortical tissue to estimate the intraneuronal tau concentration in human cortex. Using a combination of stereological counting of neurons in human cortical volume and tau concentration measurements in brain lysates by ELISA, we estimated the intraneuronal tau concentrations between 1.68 ± 0.68 μ M and 6.84 ± 0.42 μ M in the human brain (for calculations see Appendix Supplementary Methods and Appendix Tables S1–S3). This calculation intentionally underestimates the actual local concentration of tau because it does not take into account the relative concentration of tau in subcellular regions like the axon hillock and does not account for the volume of the neurons occupied by vesicular structures that lack tau, such as the rather large nucleus, mitochondria, and the ER and Golgi. Nonetheless, a p-tau441 concentration of ≈ 1.0 μ M that we found to be critical for microscopic LLPS at 10% PEG *in vitro* can thus be seen as relevant for intraneuronal tau LLPS in the human brain.

For many LLPS proteins such as the helicases Ddx4 and LAF-1 and hnRNPA1, arginine-rich positively charged sequences (e.g., RGG boxes, RRM, SR repeats) drive their LLPS in an ionic strength dependent manner (reviewed in Mitrea *et al*, 2016). Interestingly, p-tau441 droplet formation appeared to be insensitive to increasing salt conditions (≤ 1 M NaCl), suggesting that shielding of electrostatic interactions had a small effect on LLPS of p-tau441. Neither very high (pH

9.5) or low (pH 3.0) pH of the buffer, nor high concentrations (≤ 1 M) of other mono- (KCl) or bivalent (MgCl_2) cation salts did effect tau droplet formation (Fig EV3C and D). Indeed, we were able to observe droplet formation up to 3 M NaCl, whereby droplets deformed and adhered fast to the supporting glass surface at $\text{NaCl} > 1$ M (Fig 2G and H). Interestingly, p-tau441 droplet formation could be reduced and even prevented when applying chaotropic salts such as guanidinium hydrochloride (GdmHCl) and sodium thiocyanate (NaSCN) at concentrations ≥ 0.5 M (Fig 2H). Notably, 1 M GdmHCl induced tau aggregates on the glass surface, whereas 1 M NaSCN prevented visible tau droplets or aggregates. Interestingly, when adding the kosmotropic salt ammonium sulfate ($(\text{NH}_4)_2\text{SO}_4$), tau droplets became substantially larger in diameter (Fig 2H). According to the Hofmeister series of salts (Hofmeister, 1888), chaotrope salts like NaSCN can weaken the stability of proteins and protein assemblies that are stabilized by hydrophobic interactions, whereas “neutral” salts, such as NaCl and KCl, or kosmotropic salts like $(\text{NH}_4)_2\text{SO}_4$ can promote hydrophobic interactions in and between proteins (Sawyer & Puckridge, 1973). Furthermore, 1,6-hexanediol (10% w/v), an aliphatic alcohol that weakens hydrophobic interaction and can inhibit the LLPS of p-granules and stress granules (Patel *et al*, 2007; Kroschwald *et al*, 2015), also partially suppressed p-tau441 droplet formation (Fig 2I). The chaotropic salt and hexanediol sensitivity of p-tau441 phase separation could, for example, be attributed to hydrophobic interactions between short β -strands that can form in the repeat domain of the C-terminal half of tau (hexapeptide motifs PHF6* and PHF6 in the beginning of repeat 2 and 3; Von Bergen *et al*, 2005). Indeed, the addition of urea, which denatures proteins by destabilizing their secondary structure and protein folding, efficiently eliminated all droplet formation (Fig EV3E). Furthermore, we found that the C-terminal half of p-tau441 alone, p-tauCt (aa 242–441), was able to undergo phase separation in a NaCl-insensitive (≤ 1 M NaCl) manner as well (Fig EV4). Similar observations were very recently reported for the phase separation of the tau repeat domain only (Ambadipudi *et al*, 2017). To evaluate whether interactions of the repeat domain were essential for LLPS of tau, we also expressed the N-terminal (aa 1–256) half of tau441 in Sf9 cells, p-tau256, and tested its LLPS characteristics (Fig EV5, Movie EV10). In comparison with p-tau441 and p-tauCt, droplet formation of p-tau256 needed slightly higher protein (≈ 5 μM) and PEG ($\approx 10\%$) concentrations and was inhibited in buffer containing ≥ 500 mM NaCl (Fig EV4F) but not by hexanediol (Fig EV4G), thus likely driven by electrostatic interactions. These data suggest that the N-terminal half of tau contributes to the phase separation of full-length tau through electrostatic interactions. It seems unlikely but cannot be ruled out that concentrations of N-terminally truncated tau, sufficiently high for LLPS, exist in neurons, because tau is substrate for different proteases (Arai *et al*, 2005; Wang *et al*, 2010), and N-terminal fragments are commonly found in the healthy and AD brain (Fig EV4H). The disordered N-terminal projection domain [(Mukrasch *et al*, 2009); Fig 1A] harbors short serine- and proline-rich domains of low amino acid complexity (Appendix Fig S1B), which may contribute to tau LLPS behavior. Interestingly, the function of the large flexible unstructured N-terminal half (\approx amino acids 1–250) of tau is still uncertain, but it has been shown that conformational changes of the N-terminal half are involved in pathological “misfolded” forms of tau (Wolozin & Davies, 1987; Carmel *et al*, 1996; Jeganathan *et al*, 2006).

Together, these data show that tau LLPS is a phenomenon that can occur at relevant tau protein concentrations and crowding conditions. Tau LLPS seems to be driven by a complex combination of electrostatic and hydrophobic interactions.

Phosphorylation drives tau LLPS

Electrostatic forces are often predominant drivers for the LLPS of IDPs or protein domains (Mitrea *et al*, 2016). Phosphorylation introduces negative charges into proteins and changes the charge distribution and the electrostatic interactions along the polypeptide backbone, and hence also the LLPS characteristics of proteins. For example, phosphorylation regulates LLPS of nephrine (Li *et al*, 2012), FUS (Monahan *et al*, 2017), and RNA binding protein CPEB4 (Guillén-Boixet *et al*, 2016). Phosphorylation is also the major type of PTMs in tau (Morris *et al*, 2015), and more than 80 potential phosphorylation sites can be found in the amino acid sequence of tau (Reynolds *et al*, 2008).

Under normal conditions, phosphorylation at distinct sites initiates the dissociation of tau from MTs, and normal intraneuronal tau appears to be phosphorylated at different sites (Fig EV1F). To evaluate the role of phosphorylation for tau LLPS, we compared the ability of tau proteins with different degrees of phosphorylation to undergo phase separation. We tested two different p-tau441 constructs for LLPS (Fig 3A and B): (i) p-tau441 produced in Sf9 insect cells (Tepper *et al*, 2014; Mair *et al*, 2016), which carries an average of ≈ 12 phosphate groups, and for which we confirmed the presence of most reported phospho-sites by Western blot (Fig EV1G), (ii) alkaline phosphatase digested p-tau441, deP-tau441, with an average of ≈ 4 –5 phosphates. (Suggested remaining sites: pT153, pT181, pS214, pS217, pT231; Mair *et al*, 2016.) deP-tau441 dephosphorylation is indicated by a down-shift on the Western blot and the lack of immunoreactivity for PHF1 and 12e8 antibodies (Fig 3B). Both phosphorylation states (p-tau441 and deP-tau441) led to rapid droplet formation after the addition of PEG (Fig 4C; protein concentration = 2 μM , 50 mM NaCl). However, the droplet formation rate and final droplet size were lower for deP-tau441 compared to p-tau441 (Fig 3D). p-tau441 droplets reached a maximum volume of ≈ 80 μm^3 after 90 min; at longer incubation times (> 90 min), the p-tau441 droplet size decreased slightly, and the droplets started to show aggregate-like structured regions at the droplet surface and deformed from the previous spherical shape (Fig 3D, individual droplet gallery). Droplet fusion (= coalescence) did not occur at time points > 15 min. For deP-tau441, a similar trend was observed, with a maximum droplet volume of ≈ 50 μm^3 at 120 min after the addition of PEG. The observed drop in average p-tau441 and deP-tau441 droplet volume coincided with the time point of adsorption of tau droplets on the supporting glass surface, which may have caused the depletion of the larger droplets from the solution. Notably, the droplet growth depends on multiple parameters such as fusion, fission, Ostwald ripening, and gelation of the droplets. The size measurements can thus mostly be used for a qualitative statement of increased droplet formation propensity with increasing phosphorylation.

Non-phosphorylated recombinant tau441 (produced in *E. coli*) was unable to form droplets in presence of crowding agent, even after extended incubations times of 12 h. We speculated that the

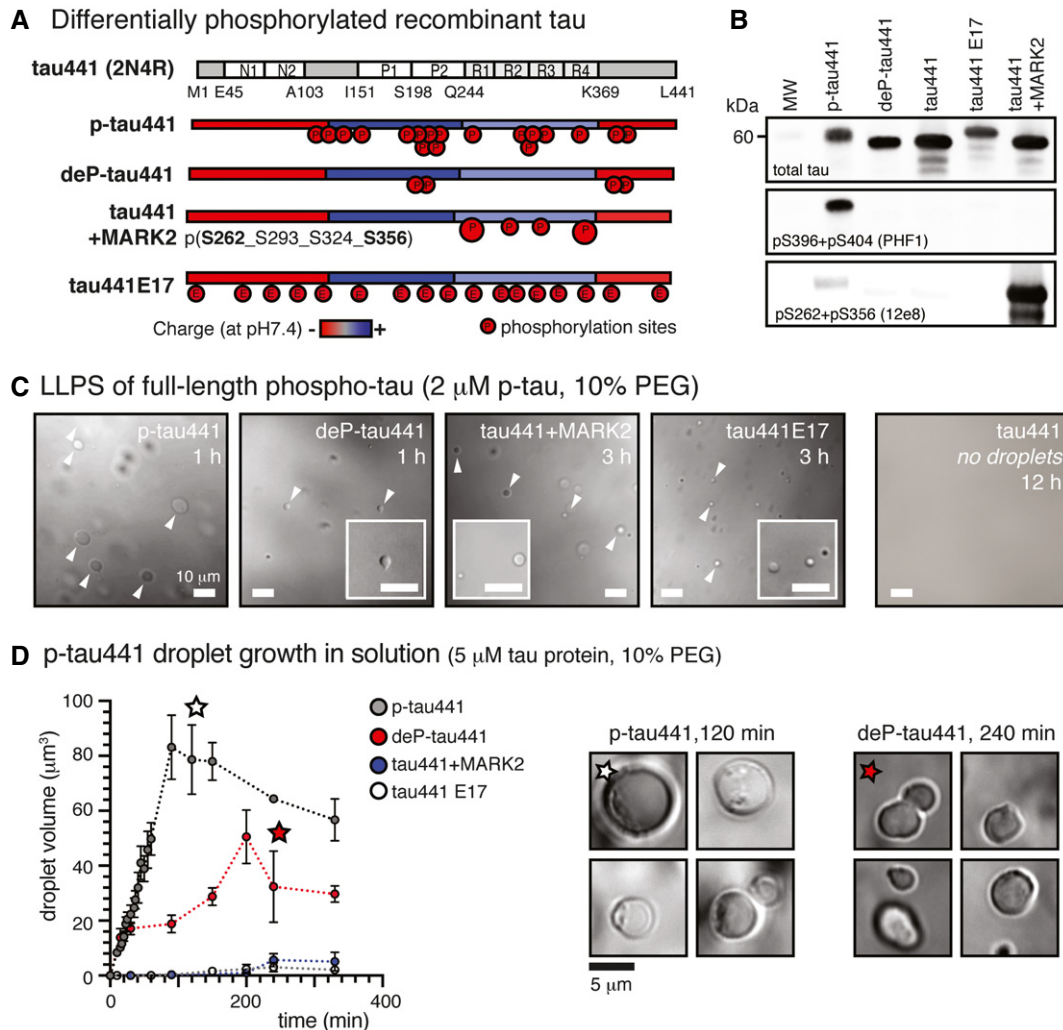


Figure 3. Phosphorylation regulates tau LLPS.

- A Scheme indicating the location of most abundant phosphorylations in the tau constructs examined: phosphorylated tau441 expressed in SF9 cells (p-tau441), dephosphorylated tau (deP-tau441) produced by alkaline phosphatase digestion of p-tau441. tau441 (produced in *Escherichia coli*) *in vitro* phosphorylated with MARK2 at indicated sites (two major and two minor sites), and phospho-mimic tau441E17 (17 glutamates at serine/threonine sites: S46, T50, T69, T111, T153, T175, T181, S199, S202, T205, T212, T217, T231, T235, S396, S404, S422) produced in *E. coli*.
- B Western blot analysis of the different phospho-tau constructs displayed in (A). Equal amounts of tau proteins were probed for phospho-epitopes pS396/pS404 (antibody PHF1) to test the phosphorylation of p-tau441 and deP-tau441 and for pS262/pS356 (antibody 12e8) to verify tau441 + MARK2 phosphorylation. tau441 and tau441E17 are not phosphorylated.
- C All phosphorylated tau constructs and the pseudo-phosphorylated tau441E17 show droplet formation (white arrows) in the presence of molecular crowding (after 3 h), whereas non-phosphorylated tau441 from *E. coli* does not.
- D Droplet growth rate and size (= spherical volume) vary between phospho-tau constructs: p-tau441 droplets grow fastest and occupy the largest volume fraction. After reaching a maximum mean droplet size, both p-tau441 and deP-tau441 both start to deform and develop “substructures” on the droplet surface. Gallery of p-tau441 and deP-tau441 droplets at indicated (red and white star) time points.

Data information: In (D), data of spherical volume and volume fraction are displayed as mean droplet volume \pm s.d., with $n = 25$ –120 droplets per condition and time point.

negative charges introduced by phosphorylation were a driving factor of tau LLPS. To test this hypothesis, we produced the phospho-mimetic mutant, tau441 E17 [=17 threonine and serine residues along the sequence of tau441 mutated into glutamate to introduce negative charges (Li *et al.*, 2011)], in *E. coli* and monitored the droplet formation. Compared to p-tau441 and deP-tau441, tau441E17 showed delayed droplet formation at

strongly reduced rates and reached small final droplet volumes ($\approx 3 \mu\text{m}^3$) and volume fractions. Moreover, by introducing minor levels of phosphorylation at specific sites in *E. coli*-derived recombinant tau441 by *in vitro* phosphorylation with kinase MARK2 (tau441 + MARK2) (Fig 3A and B), droplet formation could be rescued but at a much lower rate and with substantially smaller final droplet volumes of only $\approx 6 \mu\text{m}^3$ (Fig 3D). *In vitro* tau

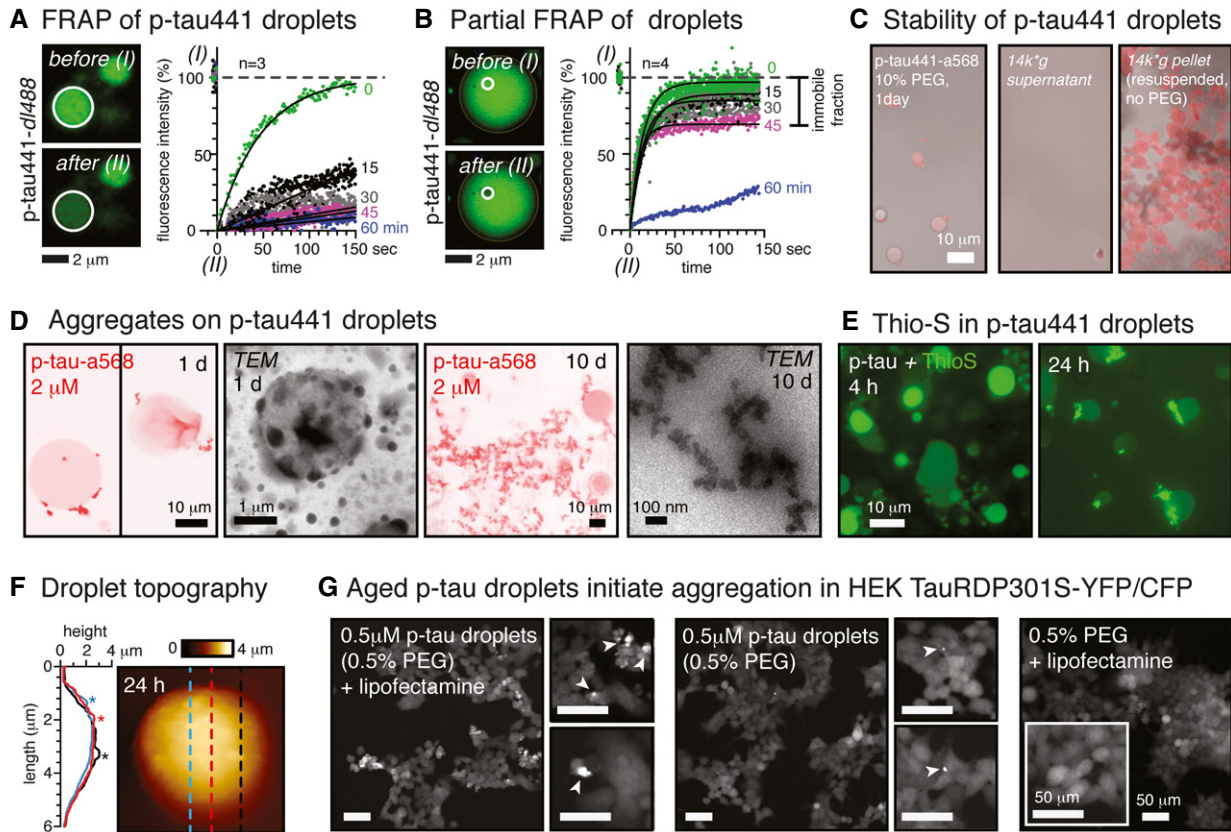


Figure 4. p-tau droplets mature and initiate tau aggregates.

A FRAP of whole droplets shows the exchange of tau molecules between droplets and the surrounding solution. When recorded at different time points after droplet initiation (0, 15, 30, 45, 60 min), whole droplet FRAP unravels that p-tau441-dl488 exchange between the droplets and the solution is efficient immediately after droplet initiation and decreases to $\sim 40\%$ after only 15 min.

B FRAP of a small fraction of the droplets is used to assess the mobility of tau molecules in the droplets. The immobile molecule fraction in the droplets increases slowly during ~ 45 min at maintained recovery rates. After 60 min, almost no p-tau441-dl488 mobility in the droplets (= no recovery) could be observed (15 μM protein; 10% dl488-labeled protein; 10% PEG).

C One-day-old p-tau441 droplets can be separated from the medium by centrifugation; they maintain droplet shape when resuspended in absence of crowding agent, indicating a gel-like polymerized texture.

D Extended incubation of p-tau441 droplets leads to formation of fibrillary tau protein aggregates in and around the droplets after 1 day; aggregates increase over time (10 days) and are visible as amorphous aggregated structures in electron microscopy.

E Thioflavin-S, which increases its fluorescence ≈ 10 -fold upon binding to β -pleated sheets in amyloid-like protein aggregates, readily co-partitions into p-tau441 droplets. After 4 h, the diffuse increase in fluorescence in some droplets may be due to the viscous droplet environment. After 24 h, ThioS fluorescence appears concentrated in tau aggregates on the droplet surface, indicating amyloid fibril cross- β structure content of these aggregates.

F Atomic force microscopy topography of 1-day-old p-tau441 droplets adsorbed to the glass surface reveals a rather high resistance of tau droplets against scanning forces of > 250 pN and the protrusion (stars in contour plots) of stable tau aggregates from the droplet surface. Height profiles (left) taken along sections indicated in the topography (right). Color scale bar on top indicates vertical height profile.

G Aged (3 days, 10 μM p-tau441 with 10% PEG at room temperature) p-tau droplets initiate tau aggregation in HEK cells expressing TauRDP301S-CFP/YFP after 10 h (0.5 μM tau with or without 0.8% lipofectamine and 0.5% PEG) (white arrows). No tau aggregation was observed in cells treated with only PEG or soluble p-tau441.

Data information: In (A, B), dots represent raw data, and lines are single exponential fits, $n = 3\text{--}4$ droplets/condition.

phosphorylation by MARK2 specifically targets two major sites (S262 and S356) and two minor sites (S293 and S324) in the repeat domain and causes the physiological detachment of tau from microtubules (Timm *et al*, 2003; Schwalbe *et al*, 2013). For both tau441E17 and tau441 + MARK2, we observed droplet coagulation but not the formation of structured regions inside the droplets or on the droplet surface.

These data indicate that pathophysiological phosphorylation of tau (as in p-tau441, Fig EV1G) as well as physiological non-pathological tau phosphorylation that detaches tau from microtubules, for

example, by MARK2, creates an electrostatic environment that can efficiently enhance the kinetics of tau LLPS. The growth rate and extent of droplet formation depended on the degree of phosphorylation, whereby the introduced negative charges (as in tau441E17) could only account for some of this effect; it seems likely that the addition of phosphate groups at certain positions is relevant for the conformational changes that can lead to LLPS of tau. The lack of tau droplet coalescence suggests a fast increase in the viscoelasticity of phospho-tau droplets preventing droplet fusion (Abbott, 1977; Gu *et al*, 2011); this is characteristic for the “maturation” of liquids into

hydrogels (Kato *et al*, 2012). The subsequent deformation of p-tau441 droplets and the formation of tau aggregates in the droplets are strong indicators for the further transition of the tau droplets from a gel-like into an aggregate state of lower energy; a similar maturation has been described for FUS (Patel *et al*, 2015). The aggregation of tau can be detected as droplet deformation and the growth of non-spherical solid aggregates.

Tau LLPS precedes aggregation *in vitro*

Liquid droplets assembled from TDP-43 (Conicella *et al*, 2016) and FUS (Burke *et al*, 2015; Patel *et al*, 2015) can transition from a reversible liquid state into a gel-like state of higher viscosity and further into amyloid-like or amorphous protein aggregates. A similar transition can lead to aberrant stress granule dynamics of C9orf72-derived dipeptide repeats, which plays a role in the pathogenesis in amyotrophic sclerosis (ALS; Taylor *et al*, 2016). In different neurodegenerative diseases such as AD and FTD, hyperphosphorylated tau is found in pathological tau aggregates (Gong *et al*, 2005), and the phosphorylation pattern of p-tau441 has been shown to be similar to that found in tau aggregates from AD brains (Mair *et al*, 2016). We next tested whether the hardening and deformation that we observed for droplets formed from phosphorylated tau describes a similar “maturation” from a liquid phase to a gel-like and finally an irreversibly aggregated state, similar to FUS and TDP-43.

To evaluate the transition from a liquid to a gel-like state, which is characterized by an increase in viscoelasticity and, hence, a decrease in molecular diffusion rates in the gel state (Kato *et al*, 2012), we performed FRAP microscopy of freshly prepared p-tau441 droplets that contained 10% of fluorescently labeled protein of the same kind (p-tau441-dl488). When bleaching the entire droplets (Fig 4A) at different times after droplet initiation (addition of 10% PEG), we found a rapid decrease of recovery in the first 15 min and virtually no recovery after 30 min. This suggested that the exchange of tau molecules between the droplets and the surrounding solution was inhibited, and indicated that the liquid droplets matured rapidly into gels of higher viscosity; this may also explain our earlier observation that p-tau441 droplet fusion was inhibited as early as after 15 min (Fig 2D). When bleaching only a small portion of a droplet to assess the molecular mobility in the droplets over time (Fig 4B), we found that the immobile fraction of molecules in p-tau441 droplets steadily increased over time to $\approx 30\%$. After 60 min, almost no FRAP was observed, which indicated the full polymerization of p-tau441 in the droplets. The progressive loss of mobile tau molecules at similar recovery rates (slope of fits) in the droplets can be explained by a progressive polymerization process of tau in the droplets, in which the amount of tau partitioning into the droplets from the medium is very limited. In contrast, a gradual droplet maturation with slowly decreasing partitioning of molecules from the surrounding medium was, for example, described for the phase transition of FUS (Shin *et al*, 2017). Our data suggest that tau droplets rapidly transition from a liquid to a gel-like state. Interestingly, the timing of full droplet maturation coincided with the droplet deformation and aggregate occurrence observed for p-tau441 (Fig 3D).

To describe the further transition toward tau aggregation, we incubated p-tau441 droplet for extended times. After 1 day of

incubation at room temperature, p-tau441 droplets were stable enough to be separated from the surrounding medium by centrifugation without losing their integrity and droplet shape, even after resuspension in buffer without PEG (Fig 4C). This indicated the maturation of the droplets into very stable gel-like spheres. Furthermore, tau protein accumulations could be found at the surface of 1-day-old p-tau441 droplets, which increased in number and size over time (Fig 4D). After 10 days, most p-tau441 droplets had transitioned into large amorphous tau aggregates. To test whether these tau aggregates contained amyloid-like β -sheet structures, we added thioflavin-S (ThioS) to fresh p-tau441 preparations and observed the fluorescence over time. ThioS is a dye that increases ≈ 10 -fold in fluorescence upon binding to β -sheet structures, which is typically used to stain amyloid-like tau protein aggregates *in vivo* and *in vitro* (Santa-María *et al*, 2006). Immediately after mixing, ThioS partitioned into p-tau441 droplets and showed only weak background fluorescence after 1 h (Fig 4E), increased fluorescence indicating β -sheets homogeneously distributed in some droplets after 4 h, and condensed β -sheet rich aggregates on droplet surfaces after 24 h.

To further explore the rigidity of the mature tau droplets, we employed atomic force microscopy (AFM). When imaging the topography of 1-day-old p-tau441 droplets (in buffer in absence of PEG) attached to a glass surface by force-distance curve-based atomic force microscopy (Dufrene *et al*, 2013), we found a rather high rigidity of the droplets, which by AFM resisted scanning forces of > 250 pN, and that small tau aggregates protruded up to ≈ 0.5 μm as stiff structures from the droplet surface (Fig 4F, Appendix Fig S3). To test whether the aggregates emerging from p-tau441 droplets were on pathway with intracellular tau aggregation, we employed a cell assay for tau aggregation, in which HEK cells expressing the FTD-mutant tau repeat domain (amino acids 243–372 of tau441) fused to CFP or YFP, TauRDP301S-CFP/YFP, were treated with preformed aged p-tau441 droplets (Fig 4G). Cells treated with 0.5 μM 3-day-old p-tau441 droplets showed TauRDP301S aggregation already after 10 h, whereas control cells that received no or non-LLPS soluble p-tau441 had no aggregates at that time point.

The rapid transition of tau droplets into a gel-like phase, the growing amount of stiff tau aggregates protruding from and filling the droplets, as well as the progressive thioflavin-S fluorescence of the droplets suggest that the conformation of tau in the droplets changes with time toward a state resembling tau β -sheet aggregates that are able to initiate intracellular tau aggregation. Together, and similar to what has been described for FUS (Patel *et al*, 2015), phospho-tau droplets undergo a maturation, whereby their fast (minutes) increase in viscoelasticity efficiently prevents droplet coalescence and initiates tau aggregation mostly on the droplet interface.

Conditions triggering tau aggregation also cause droplet formation

The *in vitro* aggregation of tau into amyloid-like fibrils has been manifold described by several authors, mostly with emphasis on aggregation kinetics and aggregate structure (von Bergen *et al*, 2000; Tepper *et al*, 2014). Most of these aggregation studies have been performed on non-phosphorylated recombinant tau (tau441), which needs the addition of polyanionic co-factors such as heparin (Goedert *et al*, 1996) or RNA (Kampers *et al*, 1996) in order to form

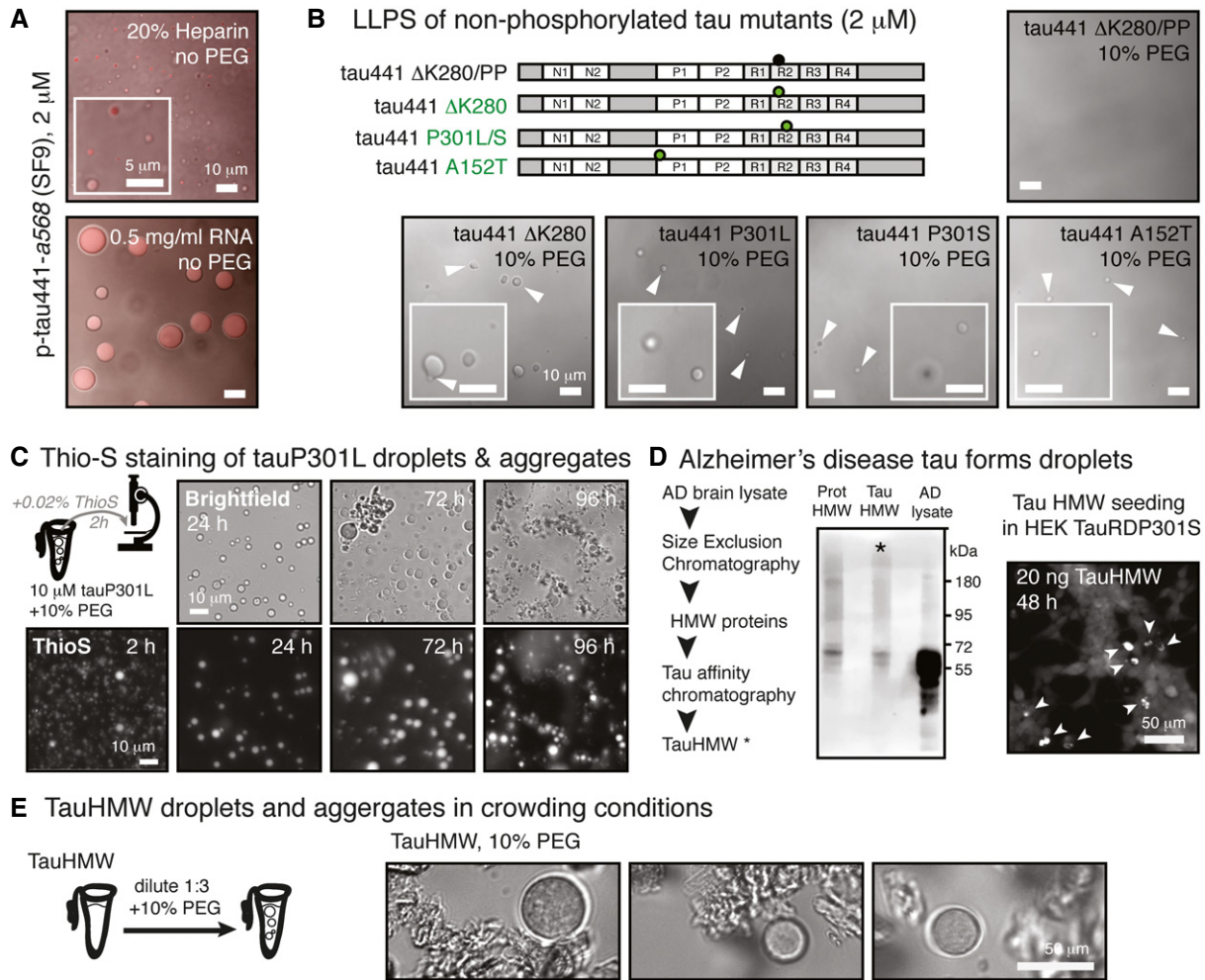


Figure 5. Factors inducing tau aggregation also lead to tau LLPS.

- A Aggregation co-factors heparin and RNA induce p-tau441 droplet formation in absence of crowding agent PEG.
- B FTD mutations (Δ K280, P301L, P301S, A152T; green circles), which trigger tau oligomerization and aggregation, can induce tau droplets (white arrows) in tau441 in absence of phosphorylation (2 μ M protein, 10% PEG). In contrast, the anti-aggregation mutant Δ K280/PP (black circle), in which two proline insertions in R2 and R3 prohibit tau repeat domain aggregation, fails to trigger tau441 LLPS.
- C Progressive aggregate formation from tauP301L droplets. Droplets of non-phosphorylated FTD-mutant tauP301L show progressive aggregate formation when incubated at room temperature; clusters of tau protein aggregates connect individual droplets after 72 h, which increased at 96 h. ThioS fluorescence in tauP301L droplets increased over time maybe due to viscosity increase, with less droplets but more ThioS-positive aggregates in the preparation after 96 h.
- D Tau (TauHMW, black asterisk in Western blot) isolated from the high molecular weight (HMW) protein fraction of Alzheimer's disease brain extract by affinity chromatography (anti-human tau antibody HT7) initiates tau aggregation (white arrowheads) in HEK TauRDP301S-CFP/YFP cells.
- E In the presence of molecular crowding (10% PEG), droplets and large aggregates can be observed in TauHMW preparations after 1–2 min.

aggregates. Because our data suggest that tau droplet formation may be on pathway with tau aggregation, we tested whether conditions triggering tau aggregation *in vitro* (pH 7.4, 50 mM salt, 20% (w/v) heparin-16000 or 0.5 mg/ml cellular RNA) also lead to LLPS. Surprisingly, we found that the addition of heparin or RNA to phosphorylated p-tau441 led to spontaneous formation of p-tau441 droplets, even in the absence of PEG (Fig 5A). We confirmed that an extended incubation of p-tau441 with heparin (data not shown), or even without (Tepper *et al*, 2014), supports the formation of fibrillary tau aggregates *in vitro*. Non-phosphorylated tau441 did not show LLPS with heparin and RNA at the same low protein concentration (2 μ M) and in the same buffer conditions.

In the context of neurodegeneration, different FTD-associated mutations in the tau gene can lead to the pathological aggregation and deposition of tau in the brain. It has been shown *in vitro* that some of these mutations enhance the nucleation and aggregation rate and enable the aggregation of recombinant tau (from *E. coli*), to some extent even in the absence of aggregation triggering co-factors (Von Bergen *et al*, 2001). The molecular mechanism behind mutation-induced tau aggregation is the strongly enhanced propensity for β -structure of the hexapeptide motif in repeat 2 (Von Bergen *et al*, 2001). To test the hypothesis that FTD mutations causing tau oligomerization and aggregation (Spillantini & Goedert, 2000) also induce tau droplet formation as a precursor of aggregation, we

mixed different non-phosphorylated (from *E. coli*) pro-aggregation mutant constructs of human full-length tau (tau441 P301L, tau441 P301S, tau441 Δ K280, tau441 A152T) with the crowding agent PEG (Fig 5B). Surprisingly, all four pro-aggregation mutants induced spontaneous droplet formation in the presence of molecular crowding, even in the absence of phosphorylation. Wild-type tau441, as well as the anti-aggregation mutant tau441 Δ K280/PP, did not undergo tau LLPS. In tau441 Δ K280/PP, the high β -propensity caused by the Δ K280 mutation is reversed by two proline insertions (I277P and I308P; Eckermann *et al*, 2007; Von Bergen *et al*, 2005). Furthermore, and similar to p-tau441 droplets, mutant tau441P301L droplets matured into aggregates and showed ThioS fluorescence (Fig 5C).

From these data, it appears that tau phase separation in solution may be a precursor of tau oligomerization and aggregation. Tau mutations, as well as phosphorylation, may favor certain protein conformations that enhance the β -strand interactions of the tau repeat domain and in turn lead to LLPS and aggregation of tau.

Tau LLPS occurs in soluble, high molecular weight tau from human AD brain

We previously showed that high molecular weight tau species, which are hyperphosphorylated and presumably oligomeric in nature, are bioactive for neuronal uptake and templated misfolding (Takeda *et al*, 2015).

To further test the idea that disease-associated soluble tau is related to LLPS and aggregation in AD, we isolated high molecular weight tau (tauHMW) from AD brain lysate by size exclusion and human tau (HT7 antibody) affinity chromatography. We found that tauHMW was able to initiate tau aggregation in HEK TauRDP301S-CFP/YFP cells (Holmes *et al*, 2014; Fig 5D), and, excitingly, showed rapid (1–2 min) phase separation into droplets as well as aggregation when applying crowding conditions (10% PEG, Fig 5E). Furthermore, by immunohistological labeling of phospho-tau in post-mortem human brain tissue with mild AD pathology (Braak stage III; Braak & Braak, 1995), we could find spherical phospho-tau accumulations in hippocampal neurons (Fig EV6). These structures were apparent in neurons with aberrant mild accumulation of p-tau in the cell body but not in neurofibrillary tangles with thioflavin-S-positive tau aggregates in the cell body; tau is normally excluded from the cell body and present only in the axon. Notably, the verification of a liquid or gel-like character of these spherical p-tau accumulations in fixed tissue cannot be assessed using the typical biophysical approaches like FRAP.

These observations are consistent with the hypothesis that hyperphosphorylated tau in AD brain can undergo LLPS and aggregation similar to what we observe for phospho-tau *in vitro*.

Discussion

While much research effort has been put toward determining tau aggregate structure, aggregation kinetics (Von Bergen *et al*, 2005), templated misfolding, and pathological toxicity of tau in the diseased brain (Walker *et al*, 2013), two extremely important questions remain unclear: What triggers the very initial aggregation of tau? And which mechanism underlies the switch from functional

soluble tau in a healthy neuron toward aberrantly pathologically folded soluble tau, and fibrillary tau accumulating in NFTs? We thought that the answer to this question may be found in two other largely unknown aspects of tau biology: in its intrinsic disorder that enables an ensemble of protein conformations and functions and in the manifold PTMs of known and unknown function. Applying multiple biophysical techniques including optical microscopy, FRAP, AFM, multiphoton imaging, and electron microscopy, we demonstrate that tau from multiple sources including recombinant tau from SF9 cells (post-translationally modified tau) and *E. coli* (unphosphorylated tau), as well as tau derived from human AD brain, (i) can undergo LLPS and (ii) that tau LLPS droplets can mature into aggregates, which may resemble the transition of soluble tau into tau aggregates in neurodegenerative diseases.

Tau is an IDP with some transient secondary structure elements of low propensity (Mukrasch *et al*, 2009). The rather short (\approx 100 aa) semi-structured repeat domain bears some transient β -sheet propensity, and its flanking proline-rich regions have been identified as relevant for microtubule binding (MTB; Mukrasch *et al*, 2007). The N-terminal half of tau stays unstructured when projecting from MTs (Chen *et al*, 1992) and, in this context, a brush of N-terminal domains on MTs may have mechanical relevance for MT spacing (Chen *et al*, 1992). Other studies showed a role of the N-terminal half of tau as binding site for kinases with SH3 domains, such as Fyn and MARK (Reynolds *et al*, 2008). Phosphorylation of tau in or next to the MT binding region, for example, by MARK, reduces the affinity of tau to microtubules and causes its detachment. Small mostly local changes in the structure of the P2 domain and short peptide stretches in the repeat domain are thought to cause the loss of tau's binding capacity to assembled MTs (Schwalbe *et al*, 2013). This process is considered a normal physiological function of tau phosphorylation that is necessary to regulate MT stability. However, hyperphosphorylation of tau often coexists with tau aggregation in the diseased brain (Augustinack *et al*, 2002; Iqbal *et al*, 2005), but the data for a causal relationship of tau aggregation to tau phosphorylation are conflicting (Kumar *et al*, 2014; Tepper *et al*, 2014; Šimić *et al*, 2016). It has been reported though that tau phosphorylation, for example, by GSK3 β at multiple sites, may precede the aggregation of tau in AD (Iqbal *et al*, 2005; Stoothoff & Johnson, 2005; Mondragón-Rodríguez *et al*, 2008). And recently, Time-Resolved ElectroSpray Ionization Mass Spectrometry (TRESI-MS) suggested a molecular conformational shift of tau toward a more amyloidogenic structure upon phosphorylation (Zhu *et al*, 2015).

Here, we suggest that LLPS of phosphorylated or mutated tau connects the somewhat enigmatic aspects of tau structural disorder, phosphorylation, and disease-relevant aggregation initiation.

Hyperphosphorylation or pro-aggregation mutations, which increase the β -sheet propensity in the repeat domain of tau and lead to tau oligomerization and aggregation (Fischer *et al*, 2007), lead to changes in the protein charge and conformation; these changes appear to be crucial for the phase separation into droplets. For example, the N-terminal half of tau (tau256), which is *a priori* zwitterionic and disordered, gains LLPS capacity when negative charges are introduced by phosphorylation in the otherwise positively charged proline-rich regions (P1 + P2), thereby neutralizing or inverting the local charge excess. Similar to other reported LLPS proteins (Brangwynne *et al*, 2015), electrostatic forces appear to be

the drivers for the LLPS of the N-terminal half of tau because it can be inhibited by increasing amounts of counter ions in solution.

In the case of full-length tau, the C-terminal half appears to introduce additional hydrophobic interactions that are sensitive to hexanediol, chaotropic salts, and protein unfolding by urea, but largely insensitive to the concentration of “simple” mono- and bivalent ions provided by NaCl, KCl, or MgCl₂ at high concentrations. Furthermore, full-length and the C-terminal half of tau seem to have the ability for LLPS at even lower protein concentrations (~1 μM) and at extremely high ion concentrations. Whether this preference for the droplet state is facilitated by hydrophobic interactions of the short hexapeptide motifs with β-strand propensity, PHF6* and PHF6 in repeat 2 and 3 of tau, remains to be clarified using high-resolution protein structural techniques. The spontaneous formation of ThioS-positive and aggregation seeding tau aggregates in and on the droplets supports this hypothesis. Furthermore, these findings are consistent with the recently reported *in vitro* LLPS of the tau repeat domain (Ambadipudi et al, 2017). Importantly, though, the contribution of the N-terminal protein half to intracellular tau LLPS has to be considered as another regulatory entity that could play an important role for either the inhibition or stabilization of LLPS in the brain.

Tau aggregates forming on the droplet surface may either consist of and grow from free soluble tau molecules in the medium, or develop due to physical properties of the droplet interface (e.g., surface tension, local tau concentration) that change the molecular properties of tau at the droplet surface and locally increase its propensity for aggregation; a similar effect is commonly utilized for the crystallization of proteins out of solution (Zhang et al, 2012), and by analogy, one could describe tau LLPS as an intracellular tau crystallization process. This idea is supported by the observation that concentrated tau solutions (> 50 μM) can spontaneously undergo LLPS even in the absence of crowding agents. Interestingly, the intracellular supersaturation of certain proteins—including tau—has recently been linked to protein aggregation and neurodegenerative diseases (Ciryam et al, 2013, 2015).

The average concentration of ≈22 μM tau we detected in the droplets is still far below the solubility limit of tau in *E. coli* and purified tau *in vitro*. Therefore, in the cell, the association of tau with other factors like polyanionic RNA, for example, in stress granules (Vanderweyde et al, 2016), or the array of tubulin C-termini on the microtubule surface (Ackmann et al, 2000) may play an important role for tau LLPS; this idea is consistent with our data showing tau LLPS induced by heparin and RNA, as well as recent independent reports from three other laboratories (Ambadipudi et al, 2017; Hernandez-Vega et al, 2017; Zhang et al, 2017).

The idea that LLPS and subsequent aggregation of tau is a fairly rapid process under physiological conditions supports our previous observation—by multiphoton *in vivo* real-time imaging—that the formation of ThioS-positive tangles in neurons of tauP301L transgenic animals can occur in the course of hours (de Calignon et al, 2010). While LLPS may not be a strict prerequisite for aggregation, since nucleation of tau aggregation has been reported, for example, from a dimeric state (Wille et al, 1992), our hypothesis that tau droplet formation can lead to tau aggregation is reinforced by the finding that the tau aggregation co-factors heparin and RNA also induce tau LLPS.

The maturation of liquid droplets into aggregates has been reported for the ALS-associated proteins FUS (Patel et al, 2015), TDP-43 (Schmidt & Rohatgi, 2016), and hnRNPA1 (Molliex et al, 2015). After LLPS, these proteins transition from an initial liquid droplet state, through a gel-like state of high viscosity, to a final stable aggregated form (Lin et al, 2015). In the case of FUS, the liquid and gel state are reversible, whereas the transition into the structurally (more) ordered aggregate state seems to be irreversible (Patel et al, 2015). Tau, in contrast to FUS, does not have a clear LCD. This structural difference may underlie the differences in biophysical properties of the resultant droplets: Our FRAP data and observations of droplet dynamics and growth can be interpreted in that tau droplets rapidly develop a “shell” of polymerized tau, which prevents the exchange of tau molecules with the surrounding medium and prohibits fusion and fission of the droplets. The inside of the droplets appears to mature into a gel phase more slowly. Upcoming *in vitro* studies using protein structure techniques will be necessary to provide insights into the molecular details of the conformational transitions underlying tau’ liquid droplet-to-aggregate transition, and *in vivo* studies will need to identify the processes that (dis)regulate tau LLPS in disease. Nonetheless, the similarity of the current data on tau to previous observations for FUS, hnRNPA1, and TDP43 indicates that the protein biophysical process of LLPS may represent a common and critical mechanism leading to ALS, AD, and FTD pathology.

Intracellular protein phase separation is used by the cell to generate transient membrane-less assemblies that fulfill certain functions; for example, stress granules assemble upon acute stress and include certain RNA binding proteins, specific RNA, and other molecules and solutes necessary to perform enhanced translation of certain genes. Protein droplets can also function as small multi-molecular machines that ensure efficient tubulin assembly (Hernández-Vega et al, 2017). We and others (Vanderweyde et al, 2016) observed droplet-like tau accumulation in neurons *in vitro* and *in vivo* in the absence of tau aggregation. This indicates a biological function of tau LLPS independent of aggregation and also suggests that healthy neurons are able to maintain tau in a potentially reversible droplet state. LLPS of full-length tau remains highly efficient even at minor amounts of phosphorylation in dephosphorylated tau (deP-tau441), and the addition of specific phosphorylation by MARK2 that causes the detachment of tau from microtubules seems sufficient to induce tau droplet formation. This further supports the idea that tau LLPS has a functional role in neurons that is in conjunction with MTB and stabilization. For example, the neuron could utilize local reversible tau LLPS to create an instantly available pool of tau in “storage droplets” at locations where microtubule polymerization is needed, such as after axon injury, at branching points, or in the growth cone. In fact, tau droplets can very efficiently induce microtubule assembly (Hernandez-Vega et al, 2017). Besides microtubule-related functions, tau droplets could interact with other polymer-gel entities in the cell (e.g., the nuclear pore complex nucleoporins) or facilitate the transport of molecules partitioning into the droplets. In fact, the liquid phase separation of the unstructured N-terminal half of tau may be related to some of the earlier observations showing a polymer-brush-like projection of the N-termini from the surface of microtubules (Vallee & Borisy, 1977; Gustke et al, 1994) as well as from fibrillary tau aggregates (Wegmann et al, 2013). These

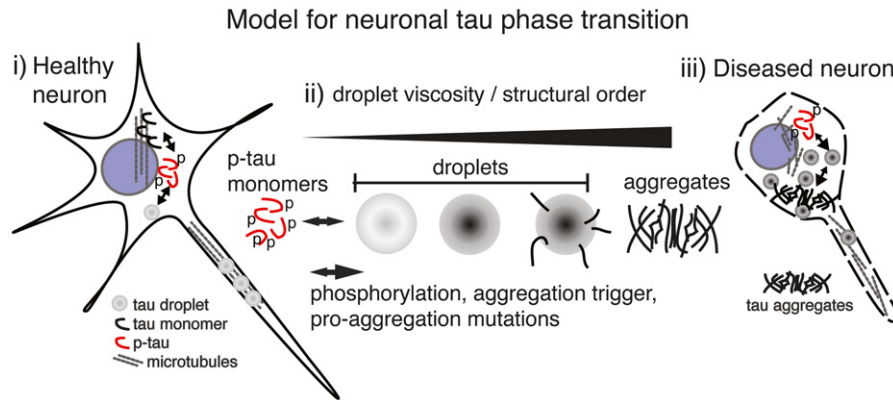


Figure 6. Tau LLPS in neurons and potential consequences in tauopathies.

In healthy neurons (i), physiological tau phosphorylation detaches tau from microtubules and can lead to intraneuronal p-tau droplets. (ii) Disease-associated hyperphosphorylation and aggregation triggering FTD mutations favor the droplet state of p-tau and lead to maturation of p-tau droplets into a viscous gel and subsequent conversion into tau aggregates that can seed further tau aggregation. In the diseased neuron (iii), stable droplets and aggregates deplete p-tau from the pool available for microtubule binding, which then can lead to uncontrolled microtubule fragmentation, the disruption of proteo-homeostasis, cell stress, and eventually neuronal death.

polymer brushes can to some extent resemble two-dimensional droplets with similar gel-like properties.

However, in an intraneuronal environment, an undefined mixture of modified, truncated, and aggregated tau species with a plethora of conformations coexist, and multiple binding partners of tau including microtubules constantly change the local concentration of tau available for LLPS. In such a scenario, the role and tuning of intracellular phase transitions of tau is likely quite complicated.

Tau LLPS: an initial step toward tau aggregation and neurodegeneration

Our data support the hypothesis that LLPS of phosphorylated tau is a cell biologically relevant event, and strongly suggest that tau droplet formation may resemble the initial step for aberrant tau aggregation in the brain (Fig 6). We propose the following model for the relevance of tau LLPS in tau aggregation: (i) Intraneuronal tau, when phosphorylated (e.g., by MARK2 kinase) and detached from microtubules, can undergo LLPS to form droplets that migrate in the cytoplasm and along the axon/projections. The transition from microtubule-bound and free soluble monomeric/dimeric tau into tau droplets is facilitated by tau phosphorylation and the normal intracellular molecular crowding. In a healthy neuron, LLPS may be a normal process of containing, condensing, and providing tau locally in the axon, and soluble and phase-separated tau exist in an equilibrium in the cytosol. (ii) Hyperphosphorylation and pro-aggregation mutations shift the equilibrium by favoring the droplet state of phospho-tau, enhancing the subsequent maturation and hardening, and seeding tau aggregation in and on tau droplets. It remains to be clarified whether phosphorylation induced tau LLPS occurs as cause or result of tau mislocalization into the somato-dendritic compartment of neurons. (iii) The intraneuronal accumulation of tau droplets and aggregated tau in the cell body (e.g., in NFTs) causes not only long-term toxicity through ER stress and UPR (Salminen *et al*, 2009), but it also depletes tau from the soluble pool that is essential to maintain microtubule stability. Tau droplets could also have other direct pathological consequences, for

example, through aberrant interaction with cellular organelles or “absorption” of RNA molecules, which would impact protein expression and homeostasis of the neuron. These effects can cause high levels of short-term and long-term stress and eventually lead to neuronal death.

In the diseased brain, however, we postulate that conditions leading to aberrant tau hyperphosphorylation could favor the kinetics of droplet formation and stabilization—such as AD and FTD (Gong *et al*, 2005), elevated oxidative stress (Alavi Naini & Soussi-Yanicostas, 2015), or traumatic brain injury (Blennow *et al*, 2012)—may favor the droplet state of tau, lead to increased droplet stability and droplet maturation, and eventually initiate tau aggregation. To what extent specific phosphorylation sites join this interplay of LLPS and aggregation remains to be explored.

Intracellular RNA (or other polyanions) may act as co-factor for tau droplet stabilization and maturation, and further experiments will have to address the specificity of RNA-induced tau LLPS (Zhang *et al*, 2017). We believe that it will be of great importance to further elucidate, (i) what are the cellular mechanisms that maintain the homeostasis of tau and other liquid phase separation proteins to prevent aggregation, (ii) whether neuronal subpopulations that are vulnerable to tau aggregation (e.g., entorhinal and hippocampal neurons in AD) also have unique tau LLPS characteristics, and (iii) whether tau droplets are able to propagate across neuronal networks and “seed” tau aggregation in connected brain areas.

Intracellular LLPS and the resulting functional membrane-less organelles, which biophysically can be described as gels or polyelectrolyte brushes, are emerging concepts in cell biology, which are now implicated in manifold cellular functions and applications (Li *et al*, 2012; Aumiller *et al*, 2014; Elbaum-Garfinkle *et al*, 2015; Jiang *et al*, 2015; Aguzzi & Altmeyer, 2016; Mitrea *et al*, 2016; Schmidt & Görlich, 2016; Schmidt & Rohatgi, 2016). For research in neurodegenerative diseases, in particular, the function and misfunction of LLPS by involved proteins—such as tau, FUS, TDP43, hnRNPA1, C9orf72 dipeptide repeats—introduces a novel exciting concept that may provide a common underlying mechanism in these diseases. Understanding the problem of initial and

progressive aggregation in AD and other protein aggregation diseases (Eftekharzadeh *et al*, 2016) may support development of novel therapeutic approaches.

Materials and Methods

Disorder, low complexity, and charge predictions

Disorder of human full-length tau [2N4R, 441 amino acids (aa)] was predicted using PONDR (<http://www.pondr.com/>) and disEMBL (<http://dis.embl.de/>), low complexity was predicted using CAST (<http://dis.embl.de/>) and SEG (<http://mendel.imp.ac.at/METHODS/seg.server.html>), and the single amino acid as well as the average (sliding window of 6 aa) charge distribution along the primary sequence was analyzed using EMBOSS (<http://www.bioinformatics.nl/cgi-bin/emboss/charge>).

Calculating the intraneuronal tau concentration in the human brain

In order to estimate the concentration of tau in neurons in the human brain, we (i) determined the number of neurons per volume in human frontal lobe cortex by stereology, then (ii) determined the amount of tau in the same cortical volume by human tau specific ELISA, and (iii) estimated the neuronal volume as either the neuronal cell body volume using previously published data (pyramidal neuron cell body diameter $\approx 20 \mu\text{m}$ = smallest possible volume; a scenario that would represent tau missorting in Alzheimer's disease), or as the space occupied by a neuron in the cortex (average cortical volume occupied per entire neuron = largest possible volume). As a result, we calculate an average intraneuronal tau concentration in the range between $1.68 \pm 0.68 \mu\text{M}$ and $6.84 \pm 0.42 \mu\text{M}$ in human frontal cortex axons. Because of a protein extraction efficiency of $\approx 23\%$, these values are likely underestimating the actual tau concentration by a factor of 4–5. Further details are presented in Appendix Supplementary Methods.

Recombinant GFP-tau expression and purification in *Escherichia coli*

Tau expression was carried out as previously reported (Barghorn *et al*, 2005). pET-29b tau plasmid containing full-length human tau tau441 (2N4R), tau mutants [tau441_E17; tau441_ΔK280; tau441_ΔK280/PP (Eckermann *et al*, 2007); tau441_P301L; tau441_P301S; and tau441_A152T (Pir *et al*, 2016)], or tau256 (N-terminal 256 amino acids of tau441) was transfected into *E. coli* BL21. For protein expression, bacteria were grown in suspension at 37°C to an optical density of 0.6 and expression was induced by adding 1 mM isopropyl beta-D-thiogalactopyranoside (IPTG) for 3.5 h. Cells were pelleted by centrifugation at 6,000 g for 20 min at 4°C and cell pellets resuspended in resuspension buffer [20 mM MES, 400 mM NaCl, 0.2 mM MgCl₂, 5 mM DTT, protease inhibitor cocktail (Complete, Roche) pH 6.8]. Cells were lysed by sonication on ice for four times 15 s on/30 s off and then boiled for 20 min. Cell debris and denatured proteins were pelleted by centrifugation at 100,000 g for 1 h at 4°C. and the supernatant was dialyzed against 1 l of ion exchange loading buffer [20 mM MES, 50 mM

NaCl, 1 mM MgCl₂, 2 mM DTT, 1 mM PMSF, pH 6.8]. Tau proteins were purified using cation exchange chromatography (column HiPrep SP FF) and size exclusion chromatography (SEC) (column Superdex G200) using an ÄKTA chromatography setup (GE Healthcare).

Recombinant tau expression and purification from Sf9

The proteins p-tau441, p-tauCt, and p-tau256 were expressed in Sf9 cells and purified as described before (Tepper *et al*, 2014). In short, the cells were infected with the recombinant virus (pVLtau40) and incubated for 3 days. The cell lysate was heated and the heat-stable tau proteins purified by size exclusion column Superdex G200 (GE Healthcare). Tau phosphorylated in Sf9 cells and then dephosphorylated (deP-tau441) was obtained as previously described (Mair *et al*, 2016) by incubating p-tau-441 (100 μl ; $\approx 5 \mu\text{M}$) with 10 U of alkaline phosphatase FAST-AP (ThermoFisher) for 20 h at 37°C in FAST-AP-Buffer. The enzyme was removed afterward by high salt treatment (incubating 10 min at 70°C, 5 M NaCl and 5 mM DTT, followed by 30 min centrifugation at 66,000 g). The protein was recovered from the supernatant by desalting (Zeba™ Desalt spin columns; Thermo Fischer). *In vitro* MARK2 phosphorylation was achieved by incubating tau441 with purified MARK2/T208V in presence of 1 mM ATP for 2 h at 37°C (Timm *et al*, 2003). The enzyme was removed by heat treatment and desalting as for deP-tau441. Phosphorylation was verified by SDS-PAGE of 0.4 μg tau protein per lane and Western blot analysis with rabbit anti-human tau (DAKO), mouse anti-phospho-tau pS262/pS356 (12e8), and mouse anti-phospho-tau p396/pS404 (PHF1, provided by Peter Davis). Phosphorylation sites previously reported in p-tau441 by mass spectrometry (Mair *et al*, 2016) were verified by Western blot with a set of antibodies against the reported sites (Fig EV1G, Appendix Table S4).

Fluorescent labeling of p-tau

p-tau256 and p-tau441 were labeled with Dylight488-NHS ester (dl488, LifeTechnologies). For highest yield of N-terminal labeling, the amino-reactive dye was dissolved in DMSO and 5 μl was added to 100 μg p-tau256 protein in PBS at pH 7.4 for 1 h at room temperature. Excess dye was removed by dialysis (SlideLizer MWCO 10 kDa, Pierce) against (10 mM HEPES buffer, 20 mM NaCl, pH 7.4) at 4°C overnight. p-tau441-a568 was produced by labeling p-tau441 using thiol-reactive AlexaFluor568 C5 maleimide (Life Technologies) according to the manual. The labeling reaction was carried out at RT for 3 h, and excess dye was removed with a NAP-5 column (GE Healthcare). In this protein, the dye can bind covalently to the two native cysteines (Cys291 and/or Cys322). In the used protein preparation, a mean [dye: protein] ratio of ~ 1.5 was achieved.

The concentration of p-tau441-a568 in the droplets was estimated from confocal images (533 nm laser line, pinhole of 3 μm). Mean droplet and background fluorescence intensity were measured from images collected at the same laser and PMT settings by measuring mean pixel intensity in ROIs using ImageJ. Fluorescence intensity was compared against images recorded in absence of LLPS from p-tau441-a568 solutions of known protein concentration. Absorbance spectrum changes of free Alexa568 in presence of

crowding agent PEG were tested using a Nanodrop and fluorescence intensity of confocal images.

Formation of tau droplets with crowding agents and polyanions

For each tested condition, the concentration of tau proteins, crowding agents [PEG-8000 or Ficoll-400 or dextran-70 (Sigma)], and different salts [NaCl, NaSCN, KCl, MgCa₂, (NH₄)₂SO₄, guanidinium hydrochloride (GdmHCl), urea (all chemicals from Sigma)] was adjusted using 10 mM HEPES pH 7.4, 10 mM citrate pH 3.0, or 10 mM Tris Base pH 9.5. All buffer solutions were degassed. Alternatively, p-tau441 LLPS was initiated by addition of RNA (total human brain RNA (0.5 µg/µl, Agilent Technologies) or 20% (w/v) heparin (MW ≈ 16,000 Da, Sigma). Control proteins bovine serum albumin (Sigma) and GFP (Abcam) were solved and then sonicated (2 × 10 s at 10% amplitude on ice) in HEPES buffer, and residual aggregates were removed by centrifugation at 21,000 g at 4°C. To visualize the droplets, 3–6 µl of the mix was immediately deposited onto a clean microscope slide and covered to avoid evaporation, or on a Matek glass-bottom dish. Imaging was performed on a Zeiss Axio-Imager microscope equipped with a CoolSnap camera, or with an Olympus FLUOVIEW confocal microscope.

To determine the droplet growth of different phospho-tau constructs, brightfield confocal z-stacks (2 µm confocal plane thickness, 20–40 µm total z-stack thickness) of free-floating droplets were recorded in the middle of the deposited solution (far above the supporting glass surface) using an Olympus FLUOVIEW confocal microscope equipped with a 63× objective. Z-stacks were recorded for each tau construct at different time points after addition of 10% PEG to 5 µM tau protein, and each experiment was repeated twice. To determine the droplet volume, only p-tau droplets in the focal plane (identified as having a thin, low-contrast droplet border) were considered. Circles were fitted on their phase border, and the droplet volume was calculated from measured circle areas in ImageJ assuming spherical droplet shape. Data are represented as mean droplet volume ± s.d.

To visualize crowding agent distribution, p-tau droplets were initiated with 9% unlabeled dextran-70 kDa and 1% dextran-3 kDa-Cascade blue, dextran-20 kDa-FITC, or dextran-70 kDa-FITC. To label tau droplets with dyes, we added 50 µM ThioS (Sigma), 100 nM methylene blue (GIBCO), or 100 nM viscous aqua (URSA Bioscience) to freshly prepared p-tau droplets.

Transmission electron microscopy

5 µl tau droplet preparations (final tau concentration ≈ 2–20 µM, 10% PEG) was directly adsorbed onto carbon-coated EM grids (Electron Microscopy Science) for 15–20 min or fixed in solution by adding 2% (w/v) paraformaldehyde (PFA) before adsorption. Excess protein was removed by placing EM grids two times on drops of fresh buffer (10 mM HEPES, 20 mM NaCl, pH 7.4), and post-fixation was done in fresh 1% (w/vol) glutaraldehyde in PBS for 3 min followed by excessive washing in water. The samples were negatively stained by incubation in 2% (w/vol) uranyl-acetate in water two times for 8 min each time, followed by brief washing in water and 10 min drying at 23°C. For immunogold labeling, polyclonal rabbit anti-tau antibody KJ9A (DAKO, antibody raised against the C-terminal half of human 4R tau) coupled with 5 nm gold particles

was added to preformed tau droplets prior to their deposition on the EM grids. Specimens were imaged by TEM (JEOL, JEM-1011, or JEM-2200FS).

Fluorescence recovery after photobleaching

fluorescence recovery after photobleaching (FRAP) experiments were performed on *in vitro* droplets formed by [p-tau256 + p-tau256-Dylight488 (9 + 1)] or [p-tau441 + p-tau441-Dylight488 (9 + 1)] using the 488 nm laser line, respectively, of a confocal Zeiss 510 microscope equipped with a 63× 1.2 NA C-APO-plan Neofluo objective (Carl Zeiss). For each droplet, either the whole droplet or a spot (diameter of ≈ 1 µm) was bleached at 100% transmission (≈ 50 mW laser power) for 2–10 s, and post-bleach time-lapse images were collected (1 s frame rate, 150 frames) and analyzed with MATLAB. For each time-lapse image, the mean fluorescence intensities of the same three regions were recorded (ROI1 = photobleached region, ROI2 = unbleached region in same droplet to correct for the overall photobleaching, and ROI3 = background signal outside of droplet was subtracted from both ROI1 and ROI2 intensities). The recovery time constant was derived from a single exponential fit of the corrected fluorescence intensities plotted versus time using GraphPad Prism 7. For FRAP of p-tau256-Dylight488 droplets in presence of RNA-Cy3, both 488 and 543 nm laser lines were used for simultaneous photobleaching of Dylight488 and Cy3 fluorophores.

Intracellular FRAP of GFP-tau441 was performed on primary cortical mouse neuron expressing GFP-tau441 or GFP-polyQ(79) (Htt exon-1 with 79Q) for 24 h or on HEK TauRDP301S-CFP/YFP cells after tau aggregation initiation using tau transgenic mouse brain lysate (details see below). For each droplet or aggregate, the bleach ROI1 was restricted to the feature of interest and bleached at 100% transmission (≈ 50 mW laser power) for 10 s, and post-bleach time-lapse images were collected (15 s frame rate, 25–30 frames) and analyzed with ImageJ. Reference ROIs were defined in the cytosol of the same cell (ROI2) and outside of the cell (ROI3).

Cloning of GFP-tau

To generate the GFP-tau441 plasmid, human full-length tau441 (2N4R) was cloned into the pMAXFP.Green (GFP) vector (Amara). GFP-tau256 was generated by adding restriction sites for KpnI and BamHI (New England Biolabs) at the 5' and 3' end, respectively, of tau256, followed by ligation into the pMAXFP.Green vector after it was digested with KpnI and BamHI. tau256 itself was generated by placing a stop codon in tau441.

Cell cultures, transfection, and droplet formation

N2a cells were cultured under standard cell culture conditions in Opti-MEM (ThermoFisher) supplemented with 10% fetal bovine serum (FBS) and 1% antibiotics penicillin/streptomycin. To express GFP-tau or GFP only, cells were transfected with plasmid DNA using Lipofectamine 2000 (ThermoFisher) according to the manufacturer's instructions and imaged 3–24 h post-transfection. Note that GFP-tau droplets were only visible in cells expressing low to medium levels of GFP-tau and before the cell body was filled with bright GFP fluorescence. Primary cortical mouse neurons were prepared from

cerebral cortices of CD1 mouse embryos (E14–15, Charles River Laboratories) using a papain dissociation system (Worthington Biochemical Corporation) as described previously (Takeda *et al*, 2015). In brief, cortices were dissected out and mechanically dissociated in Neurobasal medium (ThermoFisher) supplemented with 10% FBS, 2 mM Glutamax, 100 U/ml penicillin, and 100 g/ml streptomycin and plated in the same medium at a density of 0.6×10^5 cells per well of a Nunc™ Lab-Tek™ II Chambered Coverglass or in Chamber 1 of microfluidic devices (see below); all neuron culture dishes were previously coated with poly-D-lysine (50 mg/ml 1, Sigma). Cultures were maintained at 37°C with 5% CO₂ in Neurobasal medium with 2% (v/v) B27 nutrient, 2 mM Glutamax, and antibiotics as above. On day 7, neurons were transfected using Lipofectamine 2000. Tau droplet formation in N2a and neurons was recorded 24 h post-transfection. Imaging of live or PFA-fixed cells was performed on a confocal Zeiss 510 inverted microscope equipped with a 63× 1.2 NA C-APO-plan Neofluo objective (Carl Zeiss) and an incubation chamber to maintain culture conditions (37°C, 5% CO₂).

All animal work was performed in compliance with the MGH and NIH.

Immunofluorescence labeling and microscopy

For immunofluorescent labeling, cells were rinsed once with warm PBS and immediately fixed in 4% PFA in PBS for 10 min at RT. After washing twice with Tris-buffered saline (TBS), cells were permeabilized using 0.1% Triton X-100 in TBS for 20 min at RT, blocked in 3–5% normal goat serum (NGS) in PBS for 1 h at room temperature, and then incubated with primary antibodies (rabbit anti-Lamp1, Abcam; rabbit anti Rab5, SantaCruz; rabbit anti KDEL, Abcam; dilution 1:250 in 3% NGS/PBS) overnight at 4°C. After washing three times with TBS, secondary antibodies were applied for 1.5 h at room temperature (diluted 1:1,000 in 3% NGS/PBS), then washed off three times with PBS, and mounted with anti-fade mounting media containing DAPI. Human paraffin-embedded brain slices prepared from an old individual (88 years old, female, mild neurofibrillary tangle pathology in cortex and hippocampus, Braak stage III) were first immunolabeled as described above using a mix of rabbit phospho-tau antibodies (rabbit anti pT181, pS199, pT205, pT231, pS409; Life Technologies) and then incubated for 20 min with 0.1% (w/v) Sudan Black solution. Neurofibrillary tangles were labeled using 0.025% thioflavin-S in 50% ethanol for 8 min followed by washing with 80% ethanol for 2 min and three times water. Imaging was performed on a Zeiss Axiovert200.

Size exclusion chromatography and affinity chromatography of human brain lysates

PBS extracts of AD and control brains were Dounce homogenized (30 strokes, GKH motor drive (Glas-Col), 50% speed), spun down at 3,000 g to remove nuclei, and followed by 10,000 g to remove debris and large organelles. After filtering through a 0.2-mm membrane, 1 ml brain extract (3–4 mg total protein) was loaded onto a 12 × 1.5 cm Superdex200 prep grade SEC column (GE Healthcare) and 1.4 ml fractions were collected at a flow rate of 0.125 ml/min. Collected fractions were frozen immediately at –20°C and later analyzed for protein (BCA assay) and human tau

content by ELISA (Tau5/HT7 antibody, Calbiochem 5778010, Invitrogen MN1000B). HMW protein SEC fractions 2 + 3 from were pooled and repeatedly loaded (for 5 min at RT each load) onto a Separopore 4B-CL (bioWORLD) column coupled to mouse anti-human tau HT7 (ThermoFisher MN1000). Following three 2 ml washes, HMW tau was eluted using 1 ml of 3 M MgCl at pH 4.5. The eluted sample was dialyzed (3,500 kDa MWCO, Slide-A-Lyzer, Thermo) and then concentrated 10-fold using 3,000 kDa MWCO centrifugal filters (Amicon Ultra, Millipore). TauHMW was analyzed by standard SDS–PAGE followed by Coomassie (SimplyBlue, Invitrogen) and silver staining (Pierce 24612, Thermo Scientific), by Tau5/HT7 ELISA, and by Western blot with anti-total tau antibody (rabbit anti-human tau, DAKO). Protease inhibitor cocktail (Cell Signaling Technologies) was added to all PBS used, and extracts, buffers, and columns were kept at 4°C. Low protein binding tubes (Richell) were used whenever tau was present.

HEK cell tau aggregation assay

HEK293 cells stably expressing the repeat domain (TauRD, aa243–372) of human mutant Tau441P301S tagged with CFP and YFP (HEK TauRDP301S-CFP/YFP (Holmes *et al*, 2014)) were treated with preformed p-tau441 droplets, soluble p-tau441 [0.5 μM tau, 0.8% lipofectamine (LifeTechnologies)], or TauHMW from human AD brain lysates (20 ng tau, 0.8% lipofectamine). Treating these cells with tau material competent of seeding tau aggregation results in intracellular aggregation of TauRDP301S-CFP/YF, which can be detected as small fluorescent FRET-positive protein aggregates. Cells were imaged to evaluate the presence of aggregates after 10 or 48 h upon treatment with the tau samples. For FRAP of tau aggregates in HEK TauRDP301S-CFP/YFP, aggregation was initiated by adding brain lysate (5 μg/μl total protein) from 9-month-old human tauP301L transgenic mice [rTg4510 line (Santacruz *et al*, 2005)] to the culture medium in the presence of 1% lipofectamine 2000 (ThermoFisher) for 12 h.

Western blot analysis of cell and brain lysates and recombinant p-tau441

Intracellular phosphorylation of tau was tested by Western blot analysis of cell lysates from murine neuroblastoma N2a cells and from primary cortical mouse neurons expressing GFP-tau256 or GFP-tau441. After separation by SDS–PAGE in MES running buffer and blotting onto nitrocellulose membrane, phospho-tau in cell lysates was detected by incubating with primary antibodies (mouse anti-human tau Tau13, Biologends, 1:1,000; mouse PHF-1 (anti-pS394/pS404, Peter Davis, 1:1,000; rabbit anti p-tau mix (anti-pS199, anti-pT231, anti-pT205, Life Technologies, 1:1,000) overnight at 4°C, followed by incubation with infrared (IR) dye-labeled secondary anti-mouse680 and anti-rabbit800 antibodies (Licor) for 1 h at RT. Recombinant tau proteins which were tested for phosphorylation blots were imaged using a Licor IR scanner.

In vivo two-photon imaging of mouse cortex

An adeno-associated virus (AAV) vector encoding the fluorescent photoconvertible protein Dendra2 N-terminally fused to human

full-length tau (2N4R), AAV8-CBA-Dendra-tau441, was generated by cloning Dendra2 (Addgene) into the AAV CBA-tau441-WPRE vector. AAVs encoding Dendra2-tau441 or GFP were stereotactically injected into opposite hemispheres of wild-type mice (C57, black6, Jackson Laboratory) for expression in layer 2/3 of the somatosensory cortex (from lambda: -2.0 mm anterior/posterior, ± 2.0 mm lateral, -0.6 mm dorsal/ventral). Three weeks after injection, a cranial window was implanted by replacing a circular piece (6 mm diameter) of skull above the injection coordinates with a glass coverslip that was secured in place using dental cement and Crazy Glue.

Two-photon fluorescence of unconverted Dendra2 was excited at 800 nm using a mode-locked Ti: sapphire laser (MaiTai; Spectra Physics) and detected in the green channel (GFP emission). Image Z-stacks were recorded in anaesthetized mice using a multiphoton imaging system (Fluoview1000; Olympus; laser power, ≤ 50 mW) with a water immersion objective (25 \times , NA = 1.05; Olympus). Image processing was performed in ImageJ (National Institutes of Health).

Atomic force microscopy of droplet surface

AFM images were recorded in PBS with a BioScope Resolve microscope (Bruker) equipped with a $100 \times 100 \times 15$ μm (x, y, z) piezo-electric scanner. AFM cantilevers (PFQNM-LC from Bruker) had nominal spring constants of ≈ 0.08 N/m, had resonance frequencies of ≈ 60 kHz in buffer, and carried a SiO₂ stylus with a nominal apex radius of ≈ 65 nm. The cantilevers were functionalized with NH₂ groups, then coated with heterobifunctionalized 27-unit long PEG linkers (NHS-PEG₂₇-maleimide), and quenched with β -mercaptoethanol to lower the adhesion to imaged surfaces (Wildling *et al*, 2012). Images were taken using force-distance curve-based AFM (Dufrêne *et al*, 2013; PeakForce mode, Bruker) in buffer solution (20 mM Hepes, 50 mM NaCl, pH 7.4) at room temperature. Imaging parameters included a scan rate of 0.4–0.6 Hz, sampling rate of 2 kHz, maximum imaging force of ≈ 200 –300 pN and oscillating the AFM stylus at a vertical amplitude of ≈ 400 nm. For each topographic pixel (512 \times 512 px), the force-feedback loop limited the imaging force by regulating the stylus sample distance, which was taken to reconstruct the AFM topography. Topographs were flattened using built-in processing tools. Cross-sectional profiles were analyzed using ImageJ v1.43 (National Institutes of Health) and plotted using GraphPad Prism 7.

Expanded View for this article is available online.

Acknowledgements

We thank João Pereira for help with live-cell imaging, Jacek Biernat and Lars Krueger for helpful discussion, and the DeFiglia Lab for providing the GFP-polyQ plasmid. B.T.H. receives funding from Massachusetts Alzheimer Disease Research Center P50AG005134, J.P.T. receives funding from HHMI and NINDS R35NS097974, and E.M. and K.T. were supported by DZNE and MPG.

Author contributions

SW, BE, and KT designed and performed most experiments. BTH, JPT, EM, DM, and AAH helped with manuscript discussion. KMZ, REB, SD, PRL, DMK, TK, CC, CV, ADR, AMM, and AHV helped with experiments. ZF and SD helped with vector design and production. SW, BE, and BTH wrote the manuscript.

Conflict of interest

The authors declare that they have no conflict of interest.

References

- Abbott CE (1977) A survey of waterdrop interaction experiments. *Rev Geophys* 15: 363–374
- Ackmann M, Wiech H, Mandelkow E (2000) Nonsaturable binding indicates clustering of Tau on the microtubule surface in a paired helical filament-like conformation. *J Biol Chem* 275: 30335–30343
- Aguzzi A, Altmeyer M (2016) Phase separation: linking cellular compartmentalization to disease. *Trends Cell Biol* 26: 547–558
- Alavi Naini SM, Soussi-Yanicostas N (2015) Tau hyperphosphorylation and oxidative stress, a critical vicious circle in neurodegenerative tauopathies? *Oxid Med Cell Longev* 2015: 151979
- Ambadipudi S, Biernat J, Riedel D, Mandelkow E, Zweckstetter M (2017) Liquid–liquid phase separation of the microtubule-binding repeats of the Alzheimer-related protein Tau. *Nat Commun* 8: 275
- Arai T, Guo JP, McGeer PL (2005) Proteolysis of non-phosphorylated and phosphorylated tau by thrombin. *J Biol Chem* 280: 5145–5153
- Augustinack JC, Schneider A, Mandelkow EM, Hyman BT (2002) Specific tau phosphorylation sites correlate with severity of neuronal cytopathology in Alzheimer's disease. *Acta Neuropathol* 103: 26–35
- Aumiller WM, Davis BW, Keating CD (2014) Phase separation as a possible means of nuclear compartmentalization. *Int Rev Cell Mol Biol* 307: 109–149
- Barghorn S, Biernat J, Mandelkow E (2005) Purification of recombinant tau protein and preparation of Alzheimer-paired helical filaments *in vitro*. *Methods Mol Biol* 299: 35–51
- von Bergen M, Friedhoff P, Biernat J, Heberle J, Mandelkow EM, Mandelkow E (2000) Assembly of tau protein into Alzheimer paired helical filaments depends on a local sequence motif ((306)VQIVYK(311)) forming beta structure. *Proc Natl Acad Sci USA* 97: 5129–5134
- Berry J, Weber SC, Vaidya N, Haataja M, Brangwynne CP (2015) RNA transcription modulates phase transition-driven nuclear body assembly. *Proc Natl Acad Sci USA* 112: E5237–E5245
- Blennow K, Hardy J, Zetterberg H (2012) The neuropathology and neurobiology of traumatic brain injury. *Neuron* 76: 886–899
- Braak H, Braak E (1995) Staging of Alzheimer's disease-related neurofibrillary changes. *Neurobiol Aging* 16: 271–278
- Brangwynne CP, Eckmann CR, Courson DS, Rybarska A, Hoegge C, Gharakhani J, Julicher F, Hyman AA, Julicher F, Hyman A, Cherkasov V, Hofmann S, Druffel-Augustin S, Mogk A, Tyedmers J, Stoecklin G, Bukau B, Han T, Kato M, Xie S *et al* (2009) Germline P granules are liquid droplets that localize by controlled dissolution/condensation. *Science* 324: 1729–1732
- Brangwynne CP, Tompa P, Pappu RV (2015) Polymer physics of intracellular phase transitions. *Nat Phys* 11: 899–904
- Burke KA, Janke AM, Rhine CL, Fawzi NL (2015) Residue-by-residue view of *in vitro* FUS granules that bind the C-terminal domain of RNA polymerase II. *Mol Cell* 60: 231–241
- de Calignon A, Fox LM, Pitstick R, Carlson GA, Bacskai BJ, Spires-Jones TL, Hyman BT (2010) Caspase activation precedes and leads to tangles. *Nature* 464: 1201–1204
- Carmel G, Mager EM, Binder LI, Kuret J (1996) The structural basis of monoclonal antibody Al250's selectivity for Alzheimer's disease pathology. *J Biol Chem* 271: 32789–32795

- Chen J, Kanai Y, Cowan NJ, Hirokawa N (1992) Projection domains of MAP2 and tau determine spacings between microtubules in dendrites and axons. *Nature* 360: 674–677
- Ciryam P, Tartaglia GG, Morimoto RI, Dobson CM, Vendruscolo M (2013) Widespread aggregation and neurodegenerative diseases are associated with supersaturated proteins. *Cell Rep* 5: 781–790
- Ciryam P, Kundra R, Morimoto RI, Dobson CM, Vendruscolo M (2015) Supersaturation is a major driving force for protein aggregation in neurodegenerative diseases. *Trends Pharmacol Sci* 36: 72–77
- Conicella AE, Zerze GH, Mittal J, Fawzi NL (2016) ALS mutations disrupt phase separation mediated by α -helical structure in the TDP-43 low-complexity C-terminal domain. *Structure* 24: 1537–1549
- Drubin DG, Feinstein SC, Shooter EM, Kirschner MW (1985) Nerve growth factor-induced neurite outgrowth in PC12 cells involves the coordinate induction of microtubule assembly and assembly-promoting factors. *J Cell Biol* 101: 1799–1807
- Duf re YF, Mart nez-Mart n D, Medalsy I, Alsteens D, M ller DJ (2013) Multiparametric imaging of biological systems by force-distance curve-based AFM. *Nat Methods* 10: 847–854
- Eckermann K, Mocanu MM, Khlistunova I, Biernat J, Nissen A, Hofmann A, Sch nig K, Bujard H, Haemisch A, Mandelkow E, Zhou L, Rune G, Mandelkow EM (2007) The β -propensity of tau determines aggregation and synaptic loss in inducible mouse models of tauopathy. *J Biol Chem* 282: 31755–31765
- Eftekharzadeh B, Hyman BT, Wegmann S (2016) Structural studies on the mechanism of protein aggregation in age related neurodegenerative diseases. *Mech Ageing Dev* 156: 1–13
- Elbaum-Garfinkle S, Kim Y, Szczepaniak K, Chen CC-H, Eckmann CR, Myong S, Brangwynne CP (2015) The disordered P granule protein LAF-1 drives phase separation into droplets with tunable viscosity and dynamics. *Proc Natl Acad Sci USA* 112: 7189–7194
- Fischer D, Mukrasch MD, Von Bergen M, Klos-Witkowska A, Biernat J, Griesinger C, Mandelkow E, Zweckstetter M (2007) Structural and microtubule binding properties of tau mutants of frontotemporal dementias. *Biochemistry* 46: 2574–2582
- Fulton AB (1982) How crowded is the cytoplasm? *Cell* 30: 345–347
- Goedert M, Jakes R, Spillantini MG, Hasegawa M, Smith MJ, Crowther RA (1996) Assembly of microtubule-associated protein tau into Alzheimer-like filaments induced by sulphated glycosaminoglycans. *Nature* 383: 550–553
- Gong C-X, Liu F, Grundke-Iqbal I, Iqbal K (2005) Post-translational modifications of tau protein in Alzheimer's disease. *J Neural Transm* 112: 813–838
- Goode BL, Denis PE, Panda D, Radeke MJ, Miller HP, Wilson L, Feinstein SC (1997) Functional interactions between the proline-rich and repeat regions of tau enhance microtubule binding and assembly. *Mol Biol Cell* 8: 353–365
- Gu H, Duits MHG, Mugele F (2011) Droplets formation and merging in two-phase flow microfluidics. *Int J Mol Sci* 12: 2572–2597
- Guill n-Boixet J, Buzon V, Salvatella X, M ndez R (2016) CPEB4 is regulated during cell cycle by ERK2/Cdk1-mediated phosphorylation and its assembly into liquid-like droplets. *Elife* 5: e19298
- Gustke N, Trinczek B, Biernat J, Mandelkow EM, Mandelkow E (1994) Domains of tau protein and interactions with microtubules. *Biochemistry* 33: 9511–9522
- Hern ndez-Vega A, Braun M, Scharrel L, Jahnel M, Wegmann S, Hyman BT, Alberti S, Diez S, Hyman AA (2017) Local nucleation of microtubule bundles through tubulin concentration into a condensed tau phase. *Cell Rep* 20: 2304–2312
- Hiller G, Weber K (1978) Radioimmunoassay for tubulin: a quantitative comparison of the tubulin content of different established tissue culture cells and tissues. *Cell* 14: 795–804
- Hofmeister F (1888) Zur Lehre von der Wirkung der Salze. *Arch Exp Pathol Pharmacol* 25: 1–30
- Holmes BB, Furman JL, Mahan TE, Yamasaki TR, Mirbaha H, Eades WC, Belaygorod L, Cairns NJ, Holtzman DM, Diamond MI (2014) Proteopathic tau seeding predicts tauopathy *in vivo*. *Proc Natl Acad Sci USA* 111: E4376–E4385
- Hoover BR, Reed MN, Su J, Penrod RD, Kotilinek LA, Grant MK, Pitstick R, Carlson GA, Lanier LM, Yuan LL, Ashe KH, Liao D (2010) Tau mislocalization to dendritic spines mediates synaptic dysfunction independently of neurodegeneration. *Neuron* 68: 1067–1081
- Hyman AA, Weber CA, J licher F (2014) Liquid-liquid phase separation in biology. *Annu Rev Cell Dev Biol* 30: 39–58
- Iqbal K, Del C, Alonso A, Chen S, Chohan MO, El-Akkad E, Gong CX, Khatoon S, Li B, Liu F, Rahman A, Tanimukai H, Grundke-Iqbal I (2005) Tau pathology in Alzheimer disease and other tauopathies. *Biochim Biophys Acta* 1739: 198–210
- Jeganathan S, Von Bergen M, Brutlach H, Steinhoff HJ, Mandelkow E (2006) Global hairpin folding of tau in solution. *Biochemistry* 45: 2283–2293
- Jiang H, Wang S, Huang Y, He X, Cui H, Zhu X, Zheng Y (2015) Phase transition of spindle-associated protein regulate spindle apparatus assembly. *Cell* 163: 108–122
- Johnson GV, Stoothoff WH (2004) Tau phosphorylation in neuronal cell function and dysfunction. *J Cell Sci* 117: 5721–5729
- Kampers T, Friedhoff P, Biernat J, Mandelkow EM, Mandelkow E (1996) RNA stimulates aggregation of microtubule-associated protein tau into Alzheimer-like paired helical filaments. *FEBS Lett* 399: 344–349
- Kato M, Han TW, Xie S, Shi K, Du X, Wu LC, Mirzaei H, Goldsmith EJ, Longgood J, Pei J, Grishin NV, Frantz DE, Schneider JW, Chen S, Li L, Sawaya MR, Eisenberg D, Tycko R, McKnight SL (2012) Cell-free formation of RNA granules: low complexity sequence domains form dynamic fibers within hydrogels. *Cell* 149: 753–767
- King OD, Gitler AD, Shorter J (2012) The tip of the iceberg: RNA-binding proteins with prion-like domains in neurodegenerative disease. *Brain Res* 1462: 61–80
- Kroschwald S, Maharana S, Mateju D, Malinowska L, N se E, Poser I, Richter D, Alberti S (2015) Promiscuous interactions and protein disaggregases determine the material state of stress-inducible RNP granules. *Elife* 4: e06807
- Kumar S, Tepper K, Kaniyappan S, Biernat J, Wegmann S, Mandelkow EM, M ller DJ, Mandelkow E (2014) Stages and conformations of the Tau repeat domain during aggregation and its effect on neuronal toxicity. *J Biol Chem* 289: 20318–20332
- Lee G, Cowan N, Kirschner M (1988) The primary structure and heterogeneity of tau protein from mouse brain. *Science* 239: 285–288
- Lee K-H, Zhang P, Kim HJ, Mitrea DM, Sarkar M, Freibaum BD, Cika J, Coughlin M, Messing J, Molliex A, Maxwell BA, Kim NC, Temirov J, Moore J, Kolaitis R-M, Shaw TI, Bai B, Peng J, Kriwacki RW, Taylor JP (2016) C9orf72 dipeptide repeats impair the assembly, dynamics, and function of membrane-less organelles. *Cell* 167: 774–788
- Li X, Kumar Y, Zempel H, Mandelkow E-M, Biernat J, Mandelkow E (2011) Novel diffusion barrier for axonal retention of Tau in neurons and its failure in neurodegeneration. *EMBO J* 30: 4825–4837
- Li P, Banjade S, Cheng H-C, Kim S, Chen B, Guo L, Llaguno M, Hollingsworth JV, King DS, Banani SF, Russo PS, Jiang Q-X, Nixon BT, Rosen MK (2012)

- Phase transitions in the assembly of multivalent signalling proteins. *Nature* 483: 336–340
- Li C, Götz J (2017) Somatodendritic accumulation of Tau in Alzheimer's disease is promoted by Fyn-mediated local protein translation. *EMBO J* 36: 3120–3138
- Lim S, Haque MM, Kim D, Kim DJ, Kim YK (2014) Cell-based models to investigate Tau aggregation. *Comput Struct Biotechnol J* 12: 7–13
- Lin Y, Protter DSW, Rosen MK, Parker R (2015) Formation and maturation of phase-separated liquid droplets by RNA-binding proteins. *Mol Cell* 60: 208–219
- Lodish H, Berk A, Zipursky S (2000) Intracellular ion environment and membrane electric potential. In *Molecular cell biology*, Tenney S, Ahr K, McCaffrey P, O'Neal B, Steyn R (eds), 4th edn, pp 1–5. New York: W.H. Freeman
- Mair W, Muntel J, Tepper K, Tang S, Biernat J, Seeley WW, Kosik KS, Mandelkow E, Steen H, Steen JA (2016) FLEXITau: quantifying post-translational modifications of tau protein *in vitro* and in human disease. *Anal Chem* 88: 3704–3714
- Mitreá DM, Kriwacki RW, Handwerker KE, Cordero JA, Gall JG, Fox AH, Lamond AI, Lamond AI, Spector DL, Cioce M, Lamond AI, Brangwynne CP, Mitchison TJ, Hyman AA, Brangwynne CP, Eckmann CR, Courson DS, Rybarska A, Hoege C, Gharakhani J *et al* (2016) Phase separation in biology; functional organization of a higher order. *Cell Commun Signal* 14: 1
- Molliex A, Temirov J, Lee J, Coughlin M, Kanagaraj AP, Kim HJ, Mittag T, Taylor JP (2015) Phase separation by low complexity domains promotes stress granule assembly and drives pathological fibrillization. *Cell* 163: 123–133
- Monahan Z, Ryan VH, Janke AM, Burke KA, Rhoads SN, Zerze GH, O'Meally R, Dignon GL, Conicella AE, Zheng W, Best RB, Cole RN, Mittal J, Shewmaker F, Fawzi NL (2017) Phosphorylation of the FUS low-complexity domain disrupts phase separation, aggregation, and toxicity. *EMBO J* 36: 2951–2967
- Mondragón-Rodríguez S, Basurto-Islas G, Santa-Maria I, Mena R, Binder LI, Avila J, Smith MA, Perry G, García-Sierra F (2008) Cleavage and conformational changes of tau protein follow phosphorylation during Alzheimer's disease. *Int J Exp Pathol* 89: 81–90
- Morris M, Knudsen GM, Maeda S, Trinidad JC, Ioanoviciu A, Burlingame AL, Mucke L (2015) Tau post-translational modifications in wild-type and human amyloid precursor protein transgenic mice. *Nat Neurosci* 18: 1183–1189
- Mukrasch MD, Bibow S, Korukottu J, Jeganathan S, Biernat J, Griesinger C, Mandelkow E, Zweckstetter M (2009) Structural polymorphism of 441-residue Tau at single residue resolution. *PLoS Biol* 7: 0399–0414
- Mukrasch MD, Von Bergen M, Biernat J, Fischer D, Griesinger C, Mandelkow E, Zweckstetter M (2007) The “jaws” of the tau-microtubule interaction. *J Biol Chem* 282: 12230–12239
- Murakami T, Qamar S, Lin JQ, Schierle GSK, Rees E, Miyashita A, Costa AR, Dodd RB, Chan FTS, Michel CH, Kronenberg-Versteeg D, Li Y, Yang SP, Wakutani Y, Meadows W, Ferry RR, Dong L, Tartaglia GG, Favrin G, Lin WL *et al* (2015) ALS/FTD mutation-induced phase transition of FUS liquid droplets and reversible hydrogels into irreversible hydrogels impairs RNP granule function. *Neuron* 88: 678–690
- Nott TJ, Farber P, Petsalakis E, Jervis D, Baldwin AJ, Forman-kay JD (2014) Phase separation of disordered protein in the formation of membraneless organelles. *Biophys J* 106: 35a
- Nott TJ, Petsalaki E, Farber P, Jervis D, Fussner E, Plochowietz A, Craggs TD, Bazett-Jones DP, Pawson T, Forman-Kay JD, Baldwin AJ (2015) Phase transition of a disordered nucleic acid protein generates environmentally responsive membraneless organelles. *Mol Cell* 57: 936–947
- Patel SS, Belmont BJ, Sante JM, Rexach MF (2007) Natively unfolded nucleoporins gate protein diffusion across the nuclear pore complex. *Cell* 129: 83–96
- Patel A, Lee HO, Jawerth L, Maharana S, Jahnel M, Hein MY, Stoyanov S, Mahamid J, Saha S, Franzmann TM, Pozniakovski A, Poser I, Maghelli N, Royer LA, Weigert M, Myers EW, Grill S, Drechsel D, Hyman AA, Alberti S (2015) A liquid-to-solid phase transition of the ALS protein FUS accelerated by disease mutation. *Cell* 162: 1066–1077
- Pir GJ, Choudhary B, Mandelkow E, Mandelkow E-M (2016) Tau mutant A152T, a risk factor for FTD/PSP, induces neuronal dysfunction and reduced lifespan independently of aggregation in a *C. elegans* Tauopathy model. *Mol Neurodegener* 11: 33
- Reynolds C, Garwood C, Wray S, Price C, Kellie S, Perera T, Zvelebil M, Yang A, Sheppard P, Varndell I, Hanger D, Anderton B (2008) Phosphorylation regulates tau interactions with Src homology 3 domains of phosphatidylinositol 3-kinase, phospholipase Cgamma1, GrB2 and Src family kinases. *J Biol Chem* 283: 18177–18186
- Salminen A, Kauppinen A, Suuronen T, Kaarniranta K, Ojala J (2009) ER stress in Alzheimer's disease: a novel neuronal trigger for inflammation and Alzheimer's pathology. *J Neuroinflammation* 6: 41
- Santacruz K, Lewis J, Spires T, Paulson J, Kotilinek L, Ingelsson M, Guimaraes A, DeTure M, Ramsden M, McGowan E, Forster C, Yue M, Orne J, Janus C, Mariash A, Kuskowski M, Hyman B, Hutton M, Ashe KH (2005) Tau suppression in a neurodegenerative mouse model improves memory function. *Science* 309: 476–481
- Santa-María I, Pérez M, Hernández F, Avila J, Moreno FJ (2006) Characteristics of the binding of thioflavin S to tau paired helical filaments. *J Alzheimers Dis* 9: 279–285
- Sawyer WH, Puckridge J (1973) The dissociation of proteins by chaotropic salts. *J Biol Chem* 248: 8429–8433
- Schmidt HB, Görlich D (2016) Transport selectivity of nuclear pores, phase separation, and membraneless organelles. *Trends Biochem Sci* 41: 46–61
- Schmidt HB, Rohatgi R (2016) *In vivo* formation of vacuolated multi-phase compartments lacking membranes cell reports report *in vivo* formation of vacuolated multi-phase compartments lacking membranes. *Cell Rep* 16: 1–9
- Schwalbe M, Biernat J, Bibow S, Ozanne V, Jensen MR, Kadavath H, Blackledge M, Mandelkow E, Zweckstetter M (2013) Phosphorylation of human tau protein by microtubule affinity-regulating kinase 2. *Biochemistry* 52: 9068–9079
- Shin Y, Berry J, Pannucci N, Haataja MP, Toettcher JE, Brangwynne CP (2017) Spatiotemporal control of intracellular phase transitions using light-activated optoDroplets. *Cell* 168: 159–171.e14
- Sillen A, Leroy A, Wieruszkeski JM, Loyens A, Beauvillain JC, Buée L, Landrieu I, Lippens G (2005) Regions of tau implicated in the paired helical fragment core as defined by NMR. *ChemBioChem* 6: 1849–1856
- Šimić G, Babić Leko M, Wray S, Harrington C, Delalle I, Jovanov-Milošević N, Bažadona D, Buée L, de Silva R, Di Giovanni G, Wischik C, Hof PR (2016) Tau protein hyperphosphorylation and aggregation in Alzheimer's disease and other tauopathies, and possible neuroprotective strategies. *Biomolecules* 6: 6
- Spillantini MG, Goedert M (2000) Tau mutations in familial frontotemporal dementia. *Brain* 123(Pt 5): 857–859
- Stoothoff WH, Johnson GVW (2005) Tau phosphorylation: physiological and pathological consequences. *Biochim Biophys Acta* 1739: 280–297

- Takeda S, Wegmann S, Cho H, DeVos SL, Commins C, Roe AD, Nicholls SB, Carlson GA, Pitstick R, Nobuhara CK, Costantino I, Frosch MP, Müller DJ, Irimia D, Hyman BT (2015) Neuronal uptake and propagation of a rare phosphorylated high-molecular-weight tau derived from Alzheimer's disease brain. *Nat Commun* 6: 8490
- Taylor JP, Brown RH Jr, Cleveland DW (2016) Decoding ALS: from genes to mechanism. *Nature* 539: 197–206
- Tepper K, Biernat J, Kumar S, Wegmann S, Timm T, Hübschmann S, Redecke L, Mandelkow EM, Müller DJ, Mandelkow E (2014) Oligomer formation of tau protein hyperphosphorylated in cells. *J Biol Chem* 289: 34389–34407
- Timm T, Li XY, Biernat J, Jiao J, Mandelkow E, Vandekerckhove J, Mandelkow EM (2003) MARKK, a Ste20-like kinase, activates the polarity-inducing kinase MARK/PAR-1. *EMBO J* 22: 5090–5101
- Toretsky JA, Wright PE (2014) Assemblages: functional units formed by cellular phase separation. *J Cell Biol* 206: 579–588
- Uversky VN, Oldfield CJ, Dunker AK (2008) Intrinsically disordered proteins in human diseases: introducing the D2 concept. *Annu Rev Biophys* 37: 215–246
- Vallee RB, Borisy GG (1977) Removal of the projections from cytoplasmic microtubules *in vitro* by digestion with trypsin. *J Biol Chem* 252: 377–382
- Vanderweyde T, Apicco DJ, Youmans-Kidder K, Ash PEA, Cook C, Lummertz da Rocha E, Jansen-West K, Frame AA, Citro A, Leszyk JD, Ivanov P, Abisambra JF, Steffen M, Li H, Petrucelli L, Wolozin B (2016) Interaction of tau with the RNA-binding protein TIA1 regulates tau pathophysiology and toxicity. *Cell Rep* 15: 1455–1466
- Von Bergen M, Barghorn S, Li L, Marx A, Biernat J, Mandelkow EM, Mandelkow E (2001) Mutations of tau protein in frontotemporal dementia promote aggregation of paired helical filaments by enhancing local β -structure. *J Biol Chem* 276: 48165–48174
- Von Bergen M, Barghorn S, Biernat J, Mandelkow EM, Mandelkow E (2005) Tau aggregation is driven by a transition from random coil to beta sheet structure. *Biochim Biophys Acta* 1739: 158–166
- Walker LC, Diamond MI, Duff KE, Hyman BT (2013) Mechanisms of protein seeding in neurodegenerative diseases. *JAMA Neurol* 70: 304–310
- Wang Y, Garg S, Mandelkow E-M, Mandelkow E (2010) Proteolytic processing of tau. *Biochem Soc Trans* 38: 955–961
- Wegmann S, Medalsy ID, Mandelkow E, Müller DJ (2013) The fuzzy coat of pathological human Tau fibrils is a two-layered polyelectrolyte brush. *Proc Natl Acad Sci USA* 110: E313–E321
- Wildling L, Rankl C, Haselgrübler T, Gruber HJ, Holy M, Newman AH, Zou M-F, Zhu R, Freissmuth M, Sitte HH, Hinterdorfer P (2012) Probing binding pocket of serotonin transporter by single molecular force spectroscopy on living cells. *J Biol Chem* 287: 105–113
- Wille H, Drewes G, Biernat J, Mandelkow EM, Mandelkow E (1992) Alzheimer-like paired helical filaments and antiparallel dimers formed from microtubule-associated protein tau *in vitro*. *J Cell Biol* 118: 573–584
- Wolozin B, Davies P (1987) Alzheimer-related neuronal protein A68: specificity and distribution. *Ann Neurol* 22: 521–526
- Wright PE, Dyson HJ (2014) Intrinsically disordered proteins in cellular signalling and regulation. *Nat Rev Mol Cell Biol* 16: 18–29
- Zempel H, Mandelkow E-M (2015) Tau missorting and spastin-induced microtubule disruption in neurodegeneration: Alzheimer disease and hereditary spastic paraplegia. *Mol Neurodegener* 10: 68
- Zhang F, Roosen-Runge F, Sauter A, Roth R, Skoda MWA, Jacobs RMJ, Sztucki M, Schreiber F (2012) The role of cluster formation and metastable liquid—liquid phase separation in protein crystallization. *Faraday Discuss* 159: 313
- Zhang X, Lin Y, Eschmann NA, Zhou H, Rauch JN, Hernandez I, Guzman E, Kosik KS, Han S (2017) RNA stores tau reversibly in complex coacervates. *PLoS Biol* 15: e2002183
- Zhu S, Shala A, Bezginov A, Sljoka A, Audette G, Wilson DJ (2015) Hyperphosphorylation of intrinsically disordered tau protein induces an amyloidogenic shift in its conformational ensemble. *PLoS One* 10: e0120416



License: This is an open access article under the terms of the Creative Commons Attribution-NonCommercial-NoDerivs 4.0 License, which permits use and distribution in any medium, provided the original work is properly cited, the use is non-commercial and no modifications or adaptations are made.